AD-A146 529 WAVE-WAVE INTERACTIONS MICROSEISMS AND INFRASONIC AMBIENT NOISE IN THE OCEAN(U) TEXAS UNIV AT AUSTIN APPLIED RESEARCH LABS A C KIBBLEWHITE ET AL. 16 AUG 84 1/1

UNCLASSIFIED ARL-TR-84-2 F/G 20/1 NL

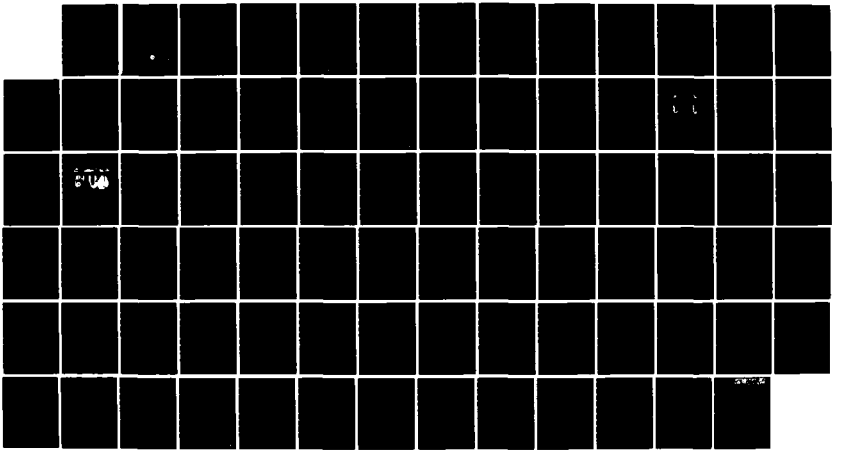

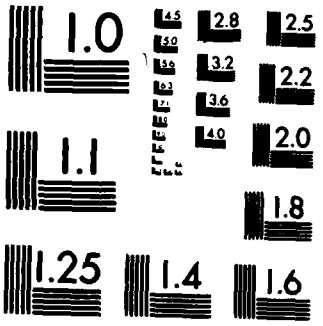
1.0
1.1
1.25
1.4
1.6
1.8
2.0
2.2
2.5
2.8
3.2
3.6
4.0
4.5
5.0
5.6

(12)

ARL-TR-84-2

Copy No. 40

WAVE-WAVE INTERACTIONS, MICROSEISMS, AND INFRASONIC AMBIENT NOISE IN THE OCEAN

Alick C. Kibblewhite
Kevin C. Ewans

APPLIED RESEARCH LABORATORIES
THE UNIVERSITY OF TEXAS AT AUSTIN
POST OFFICE BOX 8029, AUSTIN, TEXAS 78713-8029

16 August 1984

Technical Report

THIS WORK WAS SPONSORED UNDER
THE INDEPENDENT RESEARCH AND
DEVELOPMENT PROGRAM AT
APPLIED RESEARCH LABORATORIES

UNCLASSIFIED

SECURITY CLASSIFICATION OF THIS PAGE (When Data Entered)

REPORT DOCUMENTATION PAGE	READ INSTRUCTIONS BEFORE COMPLETING FORM
1. REPORT NUMBER	2. GOVT ACCESSION NO. A146329 / 3. RECIPIENT'S CATALOG NUMBER
4. TITLE (and Subtitle) WAVE-WAVE INTERACTIONS, MICROSEISMS, AND INFRASONIC AMBIENT NOISE IN THE OCEAN	5. TYPE OF REPORT & PERIOD COVERED Technical report
	6. PERFORMING ORG. REPORT NUMBER ARL-TR-84-2
7. AUTHOR(s) Alick C. Kibblewhite, Kevin C. Ewans	8. CONTRACT OR GRANT NUMBER(s)
9. PERFORMING ORGANIZATION NAME AND ADDRESS Applied Research Laboratories, The University of Texas at Austin, Austin, Texas 78713-8029	10. PROGRAM ELEMENT, PROJECT, TASK AREA & WORK UNIT NUMBERS
11. CONTROLLING OFFICE NAME AND ADDRESS	12. REPORT DATE 16 August 1984
	13. NUMBER OF PAGES 81
14. MONITORING AGENCY NAME & ADDRESS(if different from Controlling Office)	15. SECURITY CLASS. (of this report) UNCLASSIFIED
	15a. DECLASSIFICATION/DOWNGRADING SCHEDULE

16. DISTRIBUTION STATEMENT (of this Report)

Approved for public release; distribution unlimited.

17. DISTRIBUTION STATEMENT (of the abstract entered in Block 20, if different from Report)

18. SUPPLEMENTARY NOTES

This work was sponsored under the Independent Research and Development Program at Applied Research Laboratories.

19. KEY WORDS (Continue on reverse side if necessary and identify by block number)

ambient noise field
low frequencies
wave climate
ocean induced microseism
nonlinear wave-wave interactions

20. ABSTRACT (Continue on reverse side if necessary and identify by block number)

This particular work was initiated following a review of the current literature covering the ambient noise field at very low frequencies. The sparsity of good published data and the continuing interest in low frequency ambient noise have prompted this effort at this time. This report is intended to be the first in a series of contributions to the subject which will be submitted for publication in the near future from reports prepared in recent years at Applied Research Laboratories, The University of Texas (ARL:UT). In this report, correlations of wave climate and ocean induced microseism activity detected by a land-based

DD FORM 1 JAN 73 1473 EDITION OF 1 NOV 65 IS OBSOLETE

UNCLASSIFIED

SECURITY CLASSIFICATION OF THIS PAGE(When Data Entered)

20. Cont'd

sensor are examined. The quality of the data, the long term nature of the observations, and a unique property of the geographical region under investigation have helped clarify the role of nonlinear wave-wave interactions in ocean wave and ocean noise processes.

TABLE OF CONTENTS

	Page
LIST OF FIGURES	v
LIST OF TABLES	vi
I. INTRODUCTION	1
II. BACKGROUND TO THE MEASUREMENT PROGRAM	5
III. INSTRUMENTATION AND PROCEDURES	9
IV. NONLINEAR SURFACE WAVE INTERACTIONS	13
V. GENERAL RESULTS	17
A. Basic Conditions	17
B. Selected Southeasterly Events	19
1. Event 16-20 October 1981	19
2. Event 21-25 October 1981	28
VI. SPECTRAL OVERLAP AND WAVE-WAVE INTERACTIONS OF OPPOSING SEAS	31
VII. THE DEPENDENCE OF SEISMIC RESPONSE ON SEA STATE/WIND SPEED	35
VII. SPECTRAL SLOPE DEPENDENCE	39
IX. AMBIENT NOISE CHARACTERISTICS	51
A. Spectral Behavior with Wind Speed	51
B. Comparison with Other Data	53
C. Comparison with Theoretical Predictions	55
1. Noise Level	55
2. Frequency Dependence	59
D. Region Above 5 Hz	60
X. THE NONLINEAR SOURCE FUNCTION AND NOISE GENERATION	61
XI. SUMMARY	65
ACKNOWLEDGMENTS	68
REFERENCES	69

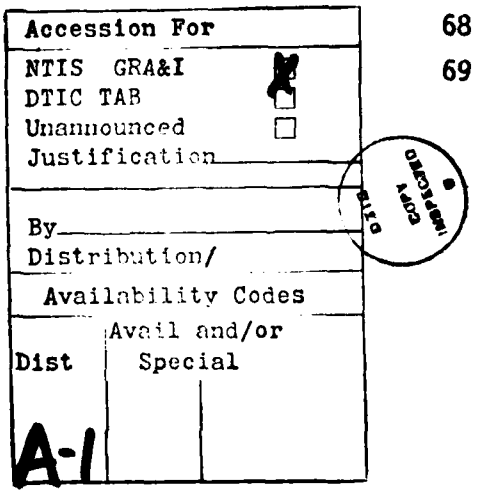

LIST OF FIGURES

Figure		Page
1	Localities and Bathymetry of Cook Strait and the Maui Environment. The Waverider buoy is installed close to the Maui platform and the receiving instrumentation ashore at Oaonui.	6
2	The History of Events for the Period 30 August 1979 - 8 September 1979	18
3	Time Series Plot of Wind, Ocean Wave, and Microseism Parameters Observed in the Maui Region, September 1979	20
4	Time Series Plot of Wind, Ocean Wave, and Microseism Parameters for the Period 16-25 October 1981. From the top: (a) Ocean wave spectral history, (b) Seismic spectral history, (c) Wind speed, m/sec, (d) Wind direction O, wave direction +, swell direction, X, (e) Significant wave height, m, (f) Average wave and microseism period, (g) Significant microseism-height, microns, (h) Wave/microseism period ratio, (i) Ratio of microseism to wave height, microns/meter.	22
5	Selected Four-Hourly Wave and Microseism Spectra for 15 October 1981	24
6	Environmental Parameters Observed in the Maui Region for the Period 16-25 March 1981	26
7	Four-Hourly Spectra for the Event on 23 October 1981	29
8	Four-Hourly Spectra for the Period 28-29 March 1981	32
9	Microseism Generation by Two Opposing Wave Fields	34

Figure		Page
10	Relationship between the Seismic and Wave Significant Heights for All Spectra in the 1980-81 Database	36
11	Relationship between the Seismic and Wave Variances of Spectra Grouped according to the Wind Direction	37
12	Logarithmic Spectra for 17 March 1981	40
13	Logarithmic Spectra for 18 March 1981	41
14	Logarithmic Spectra for 19 March 1981	42
15	Nondimensionalized Spectral Functions for the S-Group of Spectra	45
16	Ambient Noise Levels Derived from Seismic Spectra as a Function of Wind Speed	52
17	Comparison of Various Ambient Noise Data Sets	54
18	Suggested Form of the Ambient Noise Spectrum below 100 Hz in Mid-Ocean Waters	56
19	Mean "JONSWAP" Spectrum and Source Functions for the Maui Seas (Wind Speed - 15 m/sec)	62

LIST OF TABLES

I	Values of the Ratio $Su(2\omega)/[Sa(\omega)]^2$ Evaluated from the Spectral Slopes of the Nondimensional Spectra	46
II	Variation of Spectral Slope Throughout the Event 16-19 October 1981	49

I. INTRODUCTION

Studies of ambient sea noise have shown that levels in certain regions of the noise spectrum are related to local wind conditions. In his paper, Wenz[1] presented a generalized wind-dependent noise spectrum, which was supported by data from many experiments at frequencies above 200 Hz. Below 200 Hz, it was apparent that, in general, the sea noise level is controlled by non-wind related sources, such as biological, shipping, and other manmade industrial activity. However, later measurements at frequencies below 10 Hz have indicated that the wind can also have a considerable effect on noise levels in this part of the spectrum.[2]

Several mechanisms have been proposed to account for the transfer of energy from the wind to the ambient noise field at low frequencies. One of these considers that the noise source lies in turbulent pressure fluctuations in the atmospheric boundary layer.[3-7] A second considers the role of nonlinear interactions between ocean surface waves,[3,8-15] and a third examines the interaction of both surface waves and turbulence.[16] Yen and Perrone[6] provide a useful review of the basic sound generating mechanisms attributed to wind disturbance of the ocean surface.

Because reported ambient noise data are sparse at frequencies below 10 Hz, it has been difficult to assess the agreement between theory and experiment. However, a significant contribution was made recently when Nichols[17] presented new data and made comparisons with both theory and other relevant experimental results. His summarized evidence suggests that nonlinear wave-wave interactions and/or turbulence are the most likely noise generating mechanisms. While the lack of detailed environmental data did not permit definite identification, the evidence identifying the importance of nonlinear interactions appears to be growing.

For reasons outlined later, long term wave recordings have been carried out on the west coast of New Zealand to establish the general

nature and characteristics of the wave field in the area. However, because this particular region possesses certain unique features helpful to the examination of more specific ocean wave phenomena, the general program was expanded.

The particular supplementary study on which this report is based has been concerned with the role of wave-wave interactions in the generation of both wave induced microseisms and the ocean ambient noise field at very low frequencies. In spite of the vast literature on the subject,[11,18-23] debate persists as to the precise nature of the mechanism of microseism generation[18-20] and, as discussed earlier, similar ambiguity exists concerning the source of the noise field in the infrasonic region. Because nonlinear wave-wave interactions are also invoked to account for the self-stabilization of the ocean wave spectrum,[24] a parallel investigation has been concerned with the growth and decay of the ocean wave field. A third study has assessed the extent to which local sea state can be monitored using land based seismic sensors as has been done elsewhere in a less complicated environment.[25]

These studies are obviously closely related. It seemed that all might be profitably addressed in this particular geographical region through a correlation of sea state and the seismic response it generates. Existing seismic data in the range 0.1-2 Hz shows that a close relationship exists between the sound pressure at the seafloor and the seismic ground response.[21-23] Further, while the seismic amplitude spectrum will depend on both the source spectrum and the response or transfer function of the ocean/seabed system,[3] the restricted geophysical data available for this region[26] and the results of some preliminary measurements suggested that the transfer function would not unduly distort intercomparisons over the frequency range of interest. (In another study to be reported, the ocean wave and seismic measurements were supplemented by recordings of the ambient noise field; but, in the present study, no hydrophone was available.)

Much of the detail of the analysis carried out will be more appropriately reported later. However, some of the results obtained

provide a timely supplement to Nichols' review[17] and appear to justify presentation in this forum.

II. BACKGROUND TO THE MEASUREMENT PROGRAM

In 1969, a major natural gas and condensate field was discovered off the west coast of the North Island of New Zealand (Fig. 1). Because the Maui field, as it has been named, is some 30 km from the coast in water depths around 100 m, the commissioning of the field has involved a major offshore engineering operation.

In common with all modern industrial undertakings, the development of the Maui field presents a potential conflict between the material needs of society and the preservation of the environment. Through concern, as well as respect, for the environment, the company responsible for the undertaking commissioned a study of the characteristics of the Maui seas to establish any impact of the engineering operation on the region. The Maui Development Environmental Study[27] proved to be equally relevant in regard to the impact of the environment on the engineering operation.

The study involved programs in physical and chemical oceanography, coastal geology, and marine biology. A major element of the physical oceanography program has been the wave-climate investigation referred to earlier. Preliminary reports on some of the wave properties established in the early part of the program have been presented already;[28,29] but more extensive analyses, based on the larger data file which now exists, are being prepared as a new series, of which this report is one.

The preliminary analysis established that the wave field can vary significantly throughout the Maui region due to both the orographic influence of Cook Strait and to the high level, long period southwesterly swell which has its origin in the Southern Ocean.

New Zealand is subject to a regular succession of weather systems which cross the country from west to east. The mountain chain running roughly NE/SW and centered on Cook Strait acts as a barrier to the air flow associated with these systems and produces funneling effects and

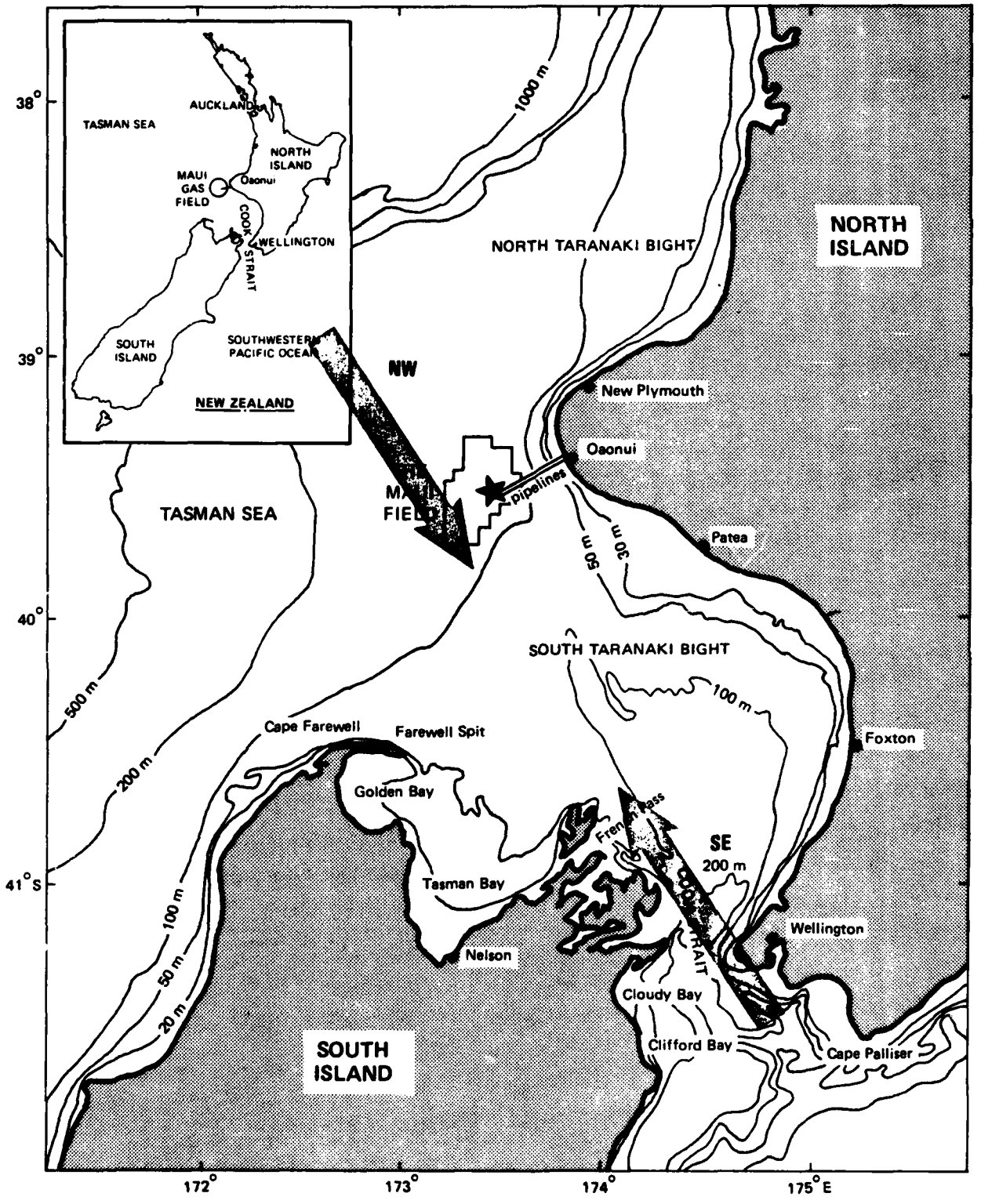

FIGURE 1
LOCALITIES AND BATHYMETRY OF THE MAUI ENVIRONMENT
WIND CHANGE ASSOCIATED WITH A SOUTHEASTERLY EVENT

ARL:UT
AS-83-1138
ACK - GA
10-25-83

strong winds in the Cook Strait and Maui region. Further, as the weather systems pass across the country, the Cook Strait area experiences well defined changes in the wind field, the wind vector often swinging quickly through approximately 180^{o} from the northwest to the southeast.

These regularly occurring southeasterly events which characterize the Maui region were early recognized as providing ideal conditions for the study of ocean wave phenomena. Not only are the wind changes well defined and repetitive, but the west coast of the North Island, just north of Cook Strait, presents an almost orthogonal coastline to the southeast winds and the overall area defines a constant fetch of approximately 200 km at the Maui platform.

III. INSTRUMENTATION AND PROCEDURES

Details of the instrumentation employed are available elsewhere[27,30] and only a brief description is given here.

The wave data were provided by a Datawell Waverider buoy (known as Maui-A) moored in approximately 110 m of water, close to the Maui platform. The signal from this unit was received on shore 30 km away and the analog output representing sea surface displacement was recorded on an instrumentation tape recorder. Also recorded were the output of a Teledyne Geotech SL210 long period seismometer installed at the receiving site, and a time code signal. Recordings of 20 min duration were initiated automatically every 4 h. In addition to the magnetically recorded data, the raw analog wave signal was processed to provide a continuous record of significant wave height and mean zero-crossing period.

Meteorological parameters for the Maui region were provided by the NZ Meteorological Service. The parameters supplied included:

(1) hourly tabulations of wind speed and direction measured with an anemometer mounted on the Maui platform,

(2) air and sea temperatures recorded at the platform by support vessels, and

(3) wave direction information as observed by the platform and its support vessels.

Spectral analysis of the magnetic tape recordings of sea surface and ground displacement was effected on a Unigon dual channel FFT processor (Model 4520) and a PDP-11 computer in two stages.

In Stage 1, the tapes were replayed into the FFT processor and the processed data transferred to the PDP-11 and stored. The wave and seismic signals were processed together.

Computed FFTs on each channel of the Unigon 4520 consist of 400 spectral estimates, the levels of which are given in decibels with respect to the sensitivity settings of the input. Each spectral estimate is an integer from 0 (-96 dB re 1 V) to 2047 (0 dB re 1 V), representing the band level (BL) of the signal. It is converted to a spectrum level (SL) according to the relation

$$SL = BL - 10 \log_{10}(BW) \quad ,$$

where BW is the bandwidth of each spectral estimate.

The frequency analysis range and playback tape speed were such that the effective frequency analysis range was 0-1 Hz with a spectral resolution of 1.17×10^{-2} Hz.

The 20 min recordings allowed an average of three consecutive maximally overlapped sweeps to be obtained. The procedure followed was to transfer each of the three average spectra to the PDP-11, scrutinize them for quality, and then compute the final spectrum as the average of these three. The spectra were then stored on file in daily lots of six spectra for Stage 2 of the analysis procedure.

Stage 2 involved spectrum scaling, parameter computation, and plotting. The raw spectra stored from Stage 1 were scaled to have units of variance density (m^2/Hz) and the following basic output parameters were computed.

(1) The number of degrees of freedom.

(2) The number of the individual spectra in the final average.

(3) The significant wave height computed from the variance of the spectrum according to the Longuet-Higgins[31] relation,

$$H_{1/3} = 4M_o^{1/2} \quad ,$$

where the nth moment M_n of the spectrum P(f) is defined as

$$M_n = \int_0^\infty f^n P(f) df \quad .$$

(4) The mean period computed from the relation

$$T_{mean} = \left[\frac{M_0}{M_2}\right]^{1/2} \quad .$$

(5) The maximum spectral estimate.

(6) The frequency of the maximum spectral estimate.

(7) The variance of the spectrum defined as the area under the spectrum,

$$\sigma^2 = \int_0^\infty P(f) df \quad .$$

(8) The spectral width parameter defined as

$$\text{Spectral Width} = \left[1 - \frac{M_2^2}{M_0 M_4}\right]^{1/2} \quad .$$

The wave and seismic spectra were plotted over the frequency bands 0.03-0.5 Hz and 0.095-1.0 Hz, respectively, and presented initially according to their GMT recording time. Various presentations were developed from this format as required.

IV. NONLINEAR SURFACE WAVE INTERACTIONS

The solution of the linearized equations of hydrodynamics produces the well known expressions for gravitational and capillary surface waves and the subsurface effects they produce. The internal disturbances, such as pressure and water particle movement, decay rapidly with depth and are negligible at a depth of the order of a wavelength. If second order terms are considered in the hydrodynamic equations, other effects appear. In particular, as first reported by Miche,[8] the generation of very low frequency pressure fluctuations due to the nonlinear interaction of opposing waves on the ocean surface can occur. The distinctive features of these waves are that the pressure effects they produce do not decrease with depth, occur at twice the surface wave frequency, and are proportional to the amplitude product of the interacting waves producing them.

Miche's theory was developed by Longuet-Higgins[9] in providing an explanation for the ocean-induced component of the microseism field. This analysis, still related to microseisms, was expanded further by Hasselmann,[3] Nanda,[10] and Darbyshire and Okeke[11] in particular. With the recent interest in the ocean ambient noise field at frequencies below 10 Hz, Miche's basic theory has also been considered by Brekhovskikh,[12] Harper and Simpkins,[13] Hughes,[14] and Lloyd[15] in seeking a theoretical basis for the observed acoustical spectrum at low frequencies and its relation to surface wind conditions.

Apart from small inconsistencies, which have been clarified by Lloyd, the theoretical predictions for the pressure field produced by nonlinear interactions are essentially the same in all treatments--Hasselmann (Ref. 3, Eq. 2.15), Brekhovskikh (Ref. 13, Eq. 53), Hughes (Ref. 14, Eq. 33), and Lloyd (Ref. 15, Eq. 35).

When the contribution from capillary waves is ignored, the expression for the one-dimensional power spectrum of the pressure field $S_p(2\omega)$ can be written in the form

$$Sp(2\omega) = 8\pi \frac{\rho^2 g^2}{c^2} \omega^3 \left[Sa(\omega)\right]^2 \int_0^{2\pi} G(\omega)\ G(\Theta+\pi) d\Theta \quad , \qquad (1)$$

where δ is the surface density of seawater, c the ocean sound velocity, ω the angular frequency of the surface wave, $Sa(\omega)$ the power spectrum level of the surface wave displacement, and the function of Θ describes the directional properties of the wave field. Following Lloyd,[15] and using the value for the integral adopted by Hughes,[14] Eq. (1) reduces to

$$Sp(2\omega) = \pi \frac{\rho^2 g^2}{c^2} \omega^3 \left[Sa(\omega)\right]^2 \quad . \qquad (2)$$

To obtain the displacement spectrum $Su(2\omega)$, relevant to the seismic measurements, the exciting pressure field must be modified by the transfer function of the layered medium so that in terms of Eq. (2)

$$Su(2\omega) = \pi \frac{\rho^2 g^2}{c^2} K_1 T_u^n(2\omega) \omega^3 \left[Sa(\omega)\right]^2 \quad , \qquad (3)$$

where K_1 is a factor involving the active area of the nonlinear interactions and the distance from the sensor, and $T_u^n(2\omega)$ is the transfer function for the vertical displacement of the elastic half space and n is the mode number.

Hasselmann[3] examines the properties of $T_u^n(2\omega)$ for a particular environmental model and gives a curve for the ratio of the effective transfer function to the transfer function for the Rayleigh mode alone, $T_u^n(2\omega)/T_u^R(2\omega)$--his Fig. 3. $T_u^R(2\omega)$ is proportional to frequency and the constant of proportionality is governed by the elastic properties of the half space. Thus, the frequency dependence of T_u^R has to be taken into account when considering absolute values. The overall frequency

dependence will depend on the shape of the curve relating T_u^n/T_u^R to the nondimensional frequency $\frac{\omega H}{2\pi c}$ (H=water depth)--see Hasselmann, Figs. 2 and 3. In the simplest case, the maximum of this ratio curve will be well above the frequency range of interest here and the simple dependence of the Rayleigh transfer function will apply. In this case, we can write

$$Su(2\omega) = \pi \frac{\rho^2 g^2}{c^2} K_1 K_2 \omega^4 \left[Sa(\omega)\right]^2 \quad , \tag{4}$$

where K_2 is a constant associated with the Rayleigh transfer function.

For this simplest case, therefore, it follows that (1) there should be a two-to-one frequency relationship between the seismic and ocean wave spectra; (2) the power spectral levels of the vertical component of the ground displacement should be proportional to the square of the power spectral levels of the ocean wavefield; and (3) the ratio $R_s = Su(2\omega)/[Sa(\omega)]^2$ should display a fourth power dependence on frequency.

In their analysis, which considers the angular distribution of the ocean surface wave field as a wave number spectrum, Yen and Perrone derive a wave number and frequency power spectrum of the pressure field (their Eq. 44) characterized by the fourth power of ω instead of the third. Evaluated in terms of the Brekhovskikh formulation, this leads to an expression for the one-dimensional frequency spectrum

$$Sp(2\omega) = 0.57 \frac{\rho^2}{c^2} \omega^6 \left[Sa(\omega)\right]^2 \int_0^{2\pi} \cos^4(\Theta) d\Theta \quad . \tag{5}$$

This is similar to Eq. (1), but implies that full consideration of the angular distribution of the wave field leads to an extra power of three in the frequency dependence.

V. GENERAL RESULTS

A. Basic Correlations

Sea wave/microseism correlations in the Maui region give clear evidence for the marine generation of microseisms in the frequency range 0.05-1.0 Hz. Comparison of any sea spectrum and its seismic equivalent will identify peaks in the wave spectrum with corresponding peaks in the microseism spectrum at or very close to twice the frequency. A primary frequency peak in the seismic spectra at the same frequency as the sea waves has also been identified in a special measurement program; but, because its level is two orders of magnitude below that of the double frequency secondary peak, it is not routinely observed in the magnetic tape recordings.

The meteorology of the western Tasman Sea controls the wave climate in the Cook Strait region and hence the microseismic response. If calm weather prevails for some time, the sea wave spectrum is then characterized by a single peak at about 0.07 Hz, produced by a persistent swell arriving from the southwest out of the Southern Ocean. The microseism spectrum has a corresponding peak at double this frequency. If a local wind then arises, it is first evident as low level broadband energy at the high frequency end of the wave spectrum. The microseism spectrum shows components at twice these frequencies. If the local sea continues to grow, the components in the sea spectrum will increase in amplitude and the associated peaks will shift to lower frequencies. If the wind persists long enough, the frequency of this peak approaches that of the long period swell and usually swamps it, the two components merging in a large peak at low frequencies. The frequency at which this occurs is often around 0.11-0.12 Hz in the wave spectrum and 0.22-0.25 Hz in the microseism spectrum. However, whereas the wave spectral levels will increase by several times during this process, the microseism levels can increase by several orders of magnitude. Figure 2 provides an example of a typical time history. It presents a time plot of significant wave heights and spectral histories for three major wave and

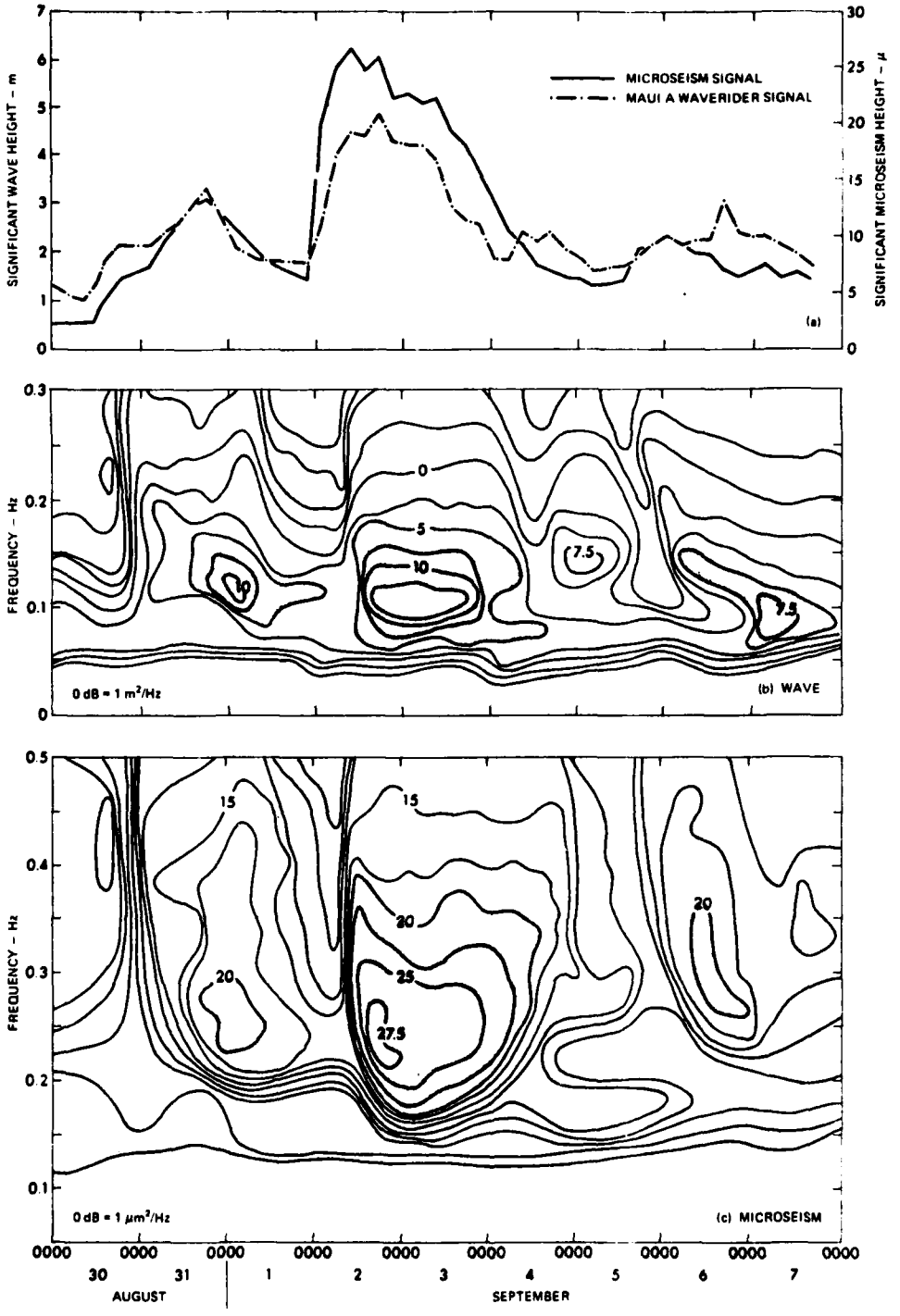

FIGURE 2
THE HISTORY OF EVENTS FOR THE PERIOD 30 AUGUST 1979 – 8 SEPTEMBER 1979

ARL:UT
BS-83-1157
ACK-GA
10-25-83

microseism generating periods; the first involves a north to northeast wind starting at 0000 h on 31 August 1979, the second a southeast wind starting at 1100 h on 2 September, and the third a westerly wind beginning at around 1800 h on 5 September. Figure 3 records the environmental parameters for this same period.

A comprehensive review of all aspects of wave/microseism behavior observed in the course of this study is presented elsewhere.[30] In this report, we restrict discussion to results relevant to identification of those effects occurring at the ocean surface, which generate the pressure field responsible for the acoustic ambient noise levels and microseisms at very low frequencies. This will lead us in particular to a discussion of periods of activity associated with southeasterly events similar to that represented by the period 2-4 September in Fig. 2.

B. Selected Southeasterly Events

In the introduction, reference was made to those features of Cook Strait which generate southeasterly (SE) meteorological events and which make this region particularly suitable for ocean wave studies. It will be instructive to develop this analysis in terms of a few such events, selected from those observed over the three-year period in which recordings have been made. While these specific events have been selected because they tell the story most clearly, the general wave/microseism behavior described is characteristic of all such events. Descriptions of others are available elsewhere.[30]

1. Event 16-20 October 1981

(a) Brief Description of the Meteorology for the Period

Over the period 13-14 October, a large anticyclone covered New Zealand. In the Maui region the winds were dominantly westerlies at around 10-15 m/sec (20-30 kt). As the anticyclone moved eastward on the 15th, the winds veered slowly north and lay in the northerly quarter

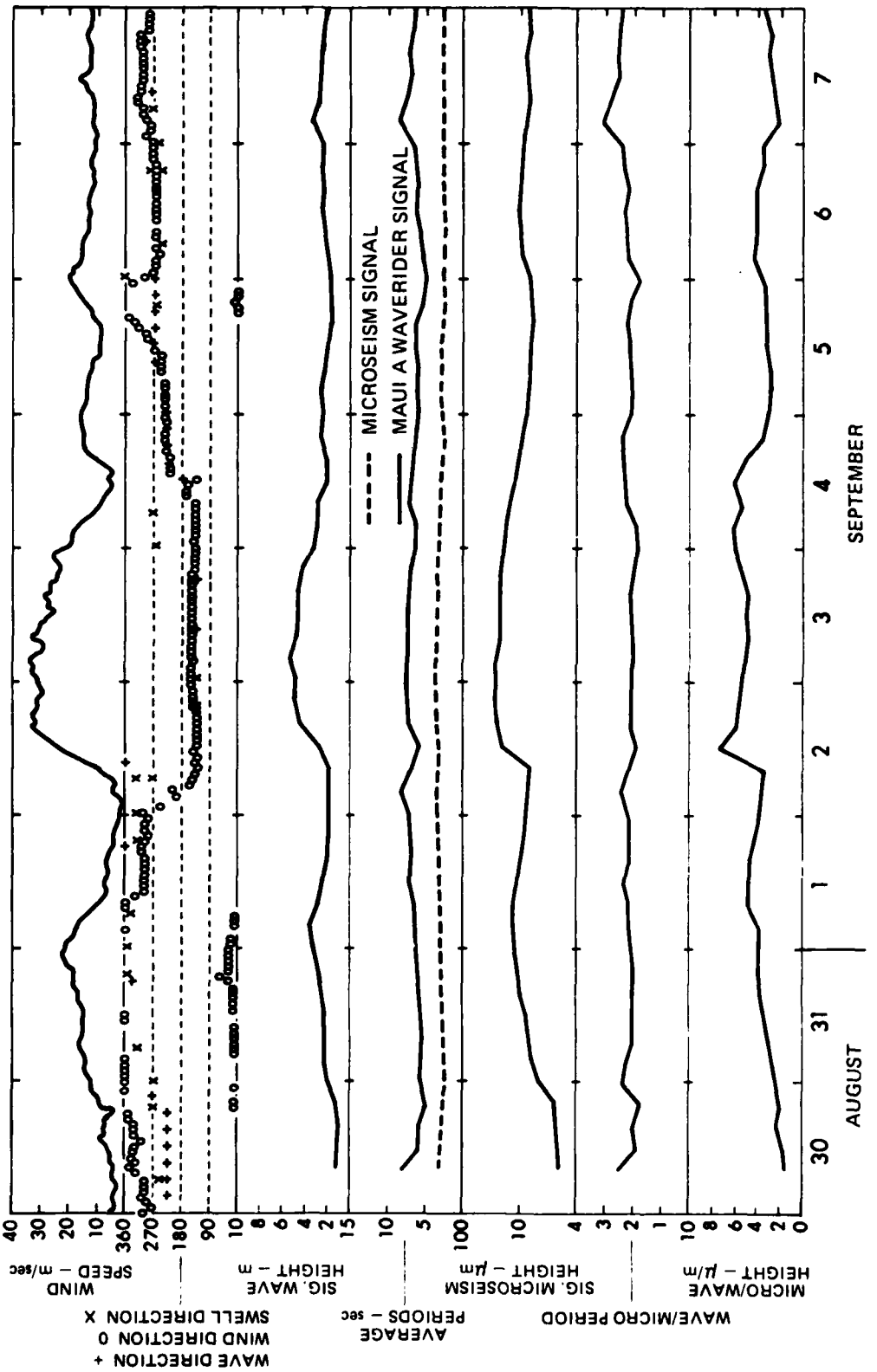

FIGURE 3
ENVIRONMENTAL PARAMETERS OBSERVED IN THE MAUI REGION, SEPTEMBER 1979

ARL:UT
AS-83-1144
ACK - GA
10 - 25 - 83

early on 16 October. During that day a low pressure system developing to the south moved rapidly onto the country. A front associated with this system crossed the Cook Strait region about midday. The wind shifted rapidly and stabilized around bearing 135°T (SE) early on 17 October (see Fig. 4). This shift in bearing was accompanied by an increase in speed to over 30 m/sec. The depression continued to move eastward over the next two days. The wind remained from the southeast, but the wind speed decreased steadily to less than 5 m/sec on 20 October, by which time another anticyclone covered the country.

Over the next few days, New Zealand was dominated by this anticyclone. The winds in the Maui region were more or less constant from the north and slowly increased to about 15 m/sec by 22 October. At this time, another low pressure system moved onto New Zealand, and the pattern of 16 October was essentially repeated. The winds again swung north and steadied once again in the southeast quarter. This change was again accompanied by an increase in wind speed (to over 30 m/sec), followed by a drop to less than 5 m/sec 24 h later.

(b) Spectral Histories of the Wave and Microseism Fields

The behavior of the ocean wave and microseism fields is best discussed in terms of the spectral contour plots for the period (Figs. 4(a),(b)).

On 14 October, the ocean wave field at the Maui platform is characterized by the low frequency swell (0.07 Hz) from the southwest and the development of a local westerly sea under the influence of the increasing westerly winds. The spectral levels of this local sea begin to decrease early on 16 October as the wind shifts slowly in bearing and decreases in intensity.

Early in the afternoon of 16 October, the spectral levels increase sharply in response to the episodic event of that day, in which the wind swings rapidly to the southeast and increases to nearly

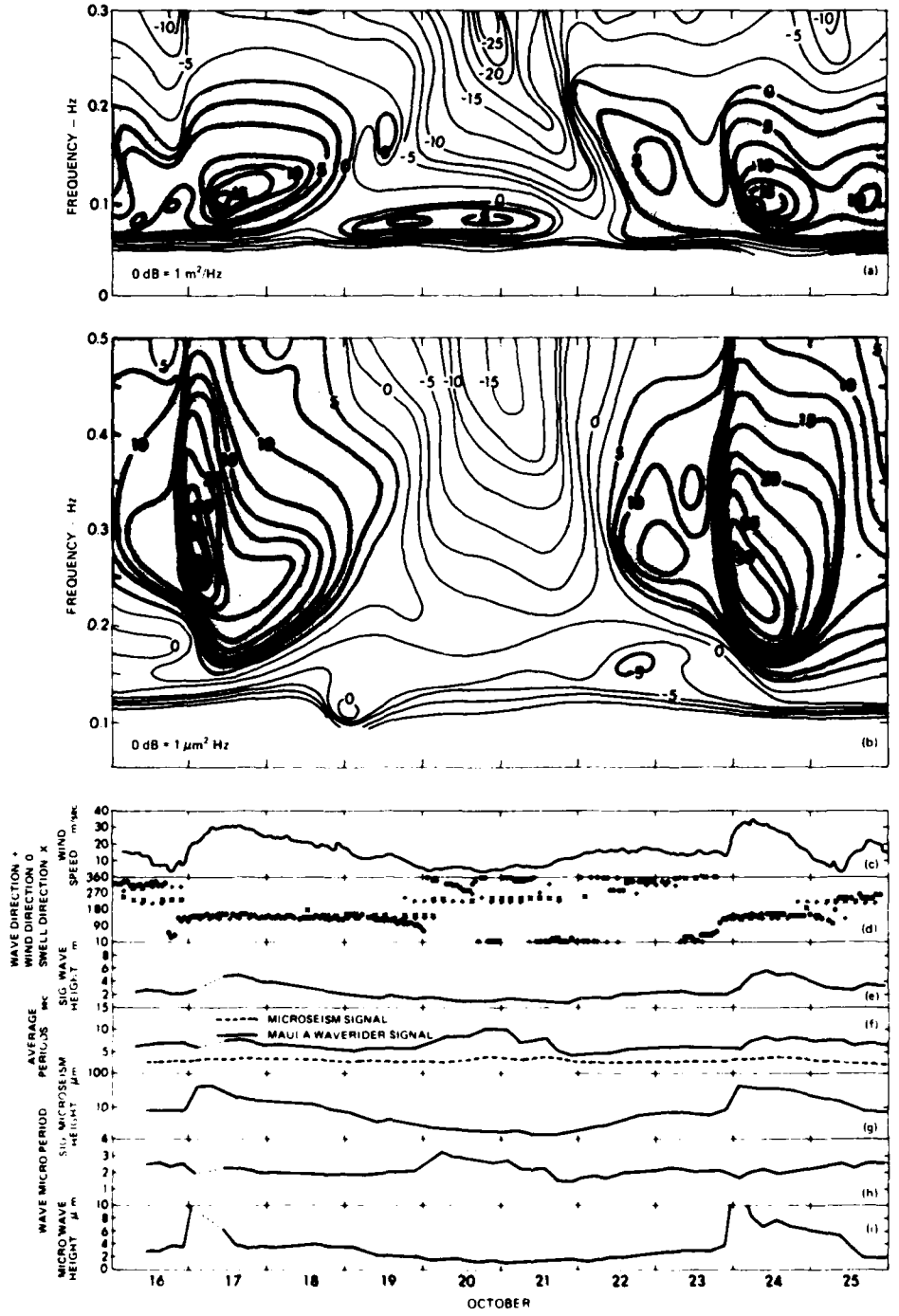

FIGURE 4
TIME HISTORY OF KEY ENVIRONMENTAL PARAMETERS FOR THE PERIOD 16-25 OCTOBER 1981

ARL:UT
BS-83-1158
ACK-GA
10-25-83

30 m/sec. A new low frequency peak in the wave spectrum has been established by midday on 17 October, and this is sufficiently strong to mask the low level southwesterly swell. Thereafter, this peak increases in frequency, and all spectral components decrease in level as the winds decrease slowly over the next three days.

Throughout 14-15 October, the microseism noise field first increases and then decays in response to the changing local westerly sea. The peak of the activity moves to lower frequencies throughout 14 October in step with the growth of the wave field, the activity extending to frequencies beyond 1 Hz. The actual four-hourly spectra for this period were quite irregular in form, a characteristic invariably found with growing and decaying wave fields (see Fig. 5). Throughout this period, the activity associated with the growing local sea dominates the microseism signal associated with the low frequency swell. The latter is nevertheless clearly apparent in the wave spectra of 15 October, but barely discernible in the microseism spectra for that time.

The wind change on 16 October produces a major and characteristic response. The initial decrease in wind speed results in a decrease in wave spectral levels. However, because of the shift in wind bearing in this interval, the seismic spectral levels increase over a broad frequency band, and then jump dramatically (by 20 dB) with the rapid increase in wind speed at 2400 h (see Fig. 4). Associated with this increase, the spectral peak moves rapidly to lower frequencies, roughly in step with the peak in the wave field. As the two spectra grow to their maximum development, they become narrower and smoother. The narrower the spectra become, the closer the spectral peaks are to an exact 2:1 frequency relationship. A close 2:1 correspondence exists by 1940Z 17 October and persists throughout the next day. Gradually, however, both the ocean wave field and seismic noise field decay in level, in response to the decreasing wind. This decay is accompanied by a shift in the spectral peaks to higher frequencies.

The significance of the shift in wind bearing during a southeasterly event is brought out clearly in the plot of the

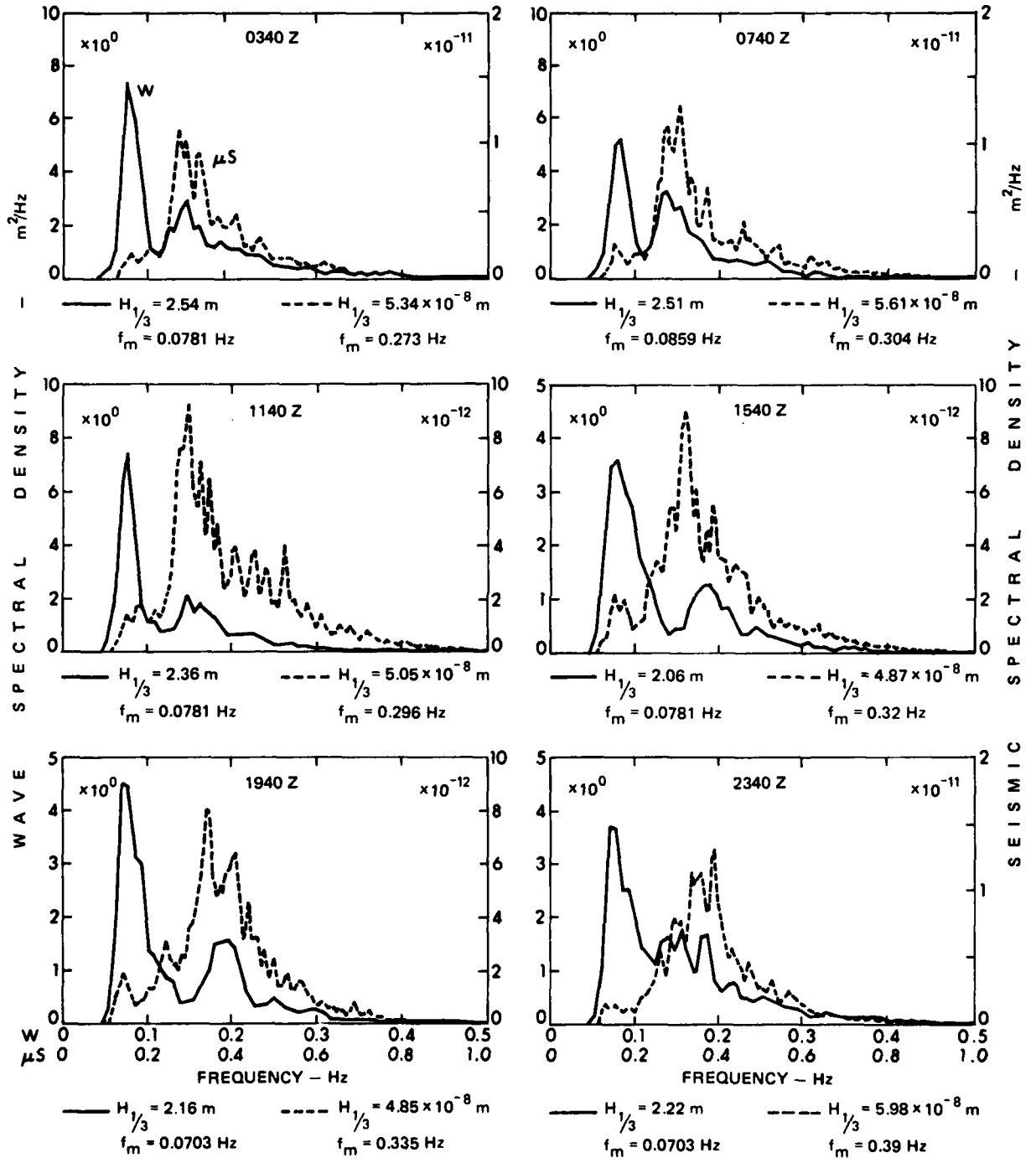

FIGURE 5
FOUR-HOURLY SPECTRA FOR 15 OCTOBER 1981

ARL:UT
AS-83-1145
ACK · GA
10 · 25 · 83

environmental parameters in Fig. 4. In particular, the ratio of the microseism/wave activity (Fig. 4(i)) shows a pronounced peak at this time. Another example occurs with the event on 23 October in the same figure, and in the other selected example from March 1981 shown in Fig. 6.

The joint behavior of the two fields can be interpreted in terms of wave-wave interactions. The rapid increase in wind speed (to approximately 30 m/sec) and change in bearing from northwest to southeast (approximately 180^{0}) brings a rapidly developing southeasterly sea into direct opposition to the original high level sea from the northwest (significant wave height is approximately 3 m, see Fig. 4(e)). Moreover, as the generating area for the latter covered a large part of the north Tasman Sea, it could be expected to persist for some time in spite of the strength of the opposing southeasterly winds. A classic situation therefore exists for the production of wave-wave interactions of the type envisaged by Brekhovskikh *and others*, *and* the generation of the associated pressure field.

The very intense microseism activity apparent in the initial part of the event of 17 October is considered to be the direct result of the interaction of the two opposing seas. Microseism spectral power levels reached the order of 10^{-9} m^2/Hz during the early part of such episodic events, and at such times the power ratio of the spectral maxima $\left[Su(2\omega)/Sa(\omega)\right]_m$ was typically 200-300 $(microns/meter)^2$. The regular occurrence of these events in the present investigation and the repetitive behavior involved give confidence in this interpretation.

In the event of 17 October, the high seismic activity drops rapidly to lower steady levels at frequencies above 0.25 Hz at around 0800. The wind reaches its highest speed at about this time and the southeasterly sea its maximum development. It is believed that this decrease in seismic noise level, which occurs without any corresponding change in the local wave spectral levels, reflects the demise of the initial northwest sea and a sharp decline in this form of wave-wave interaction.

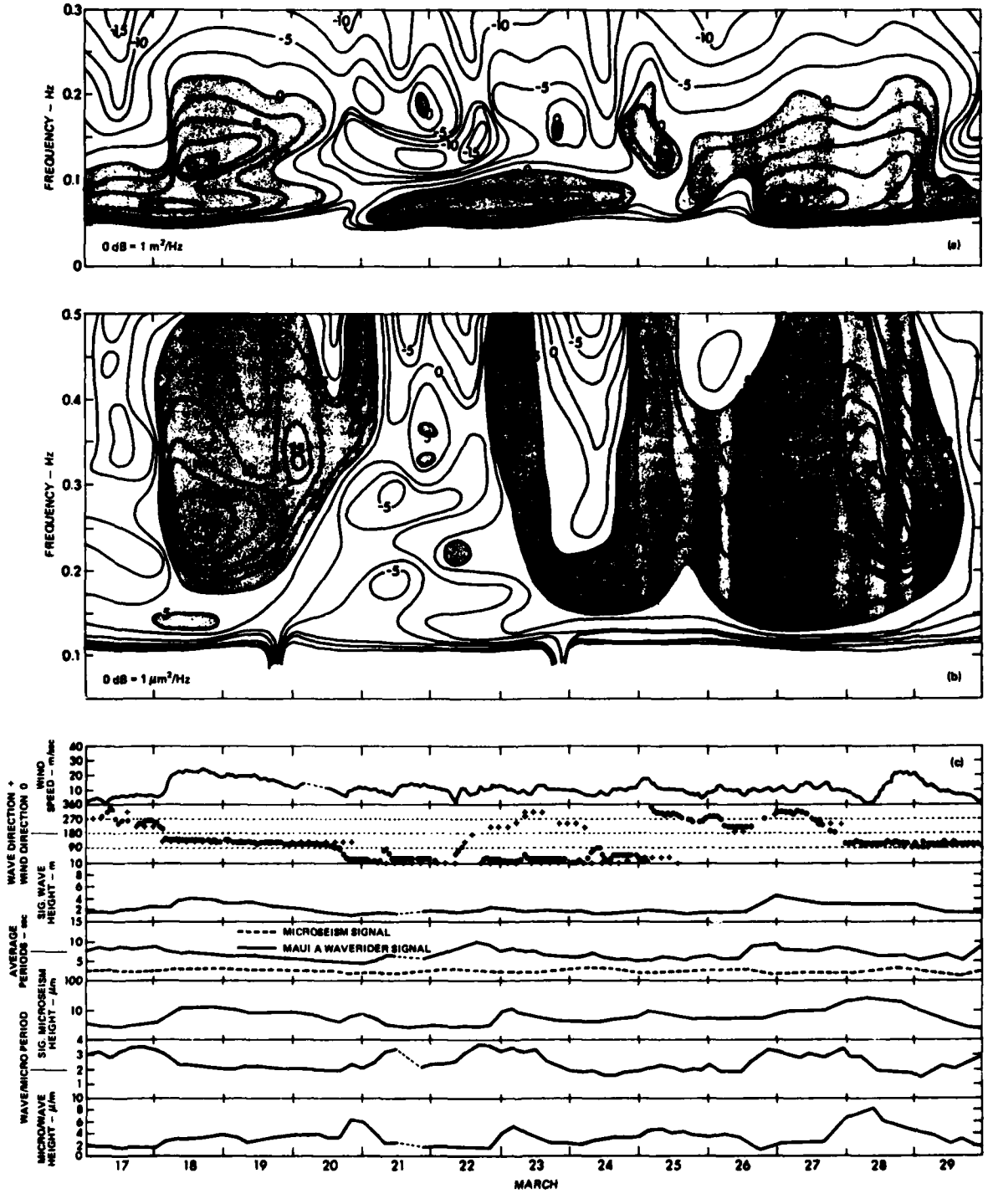

FIGURE 6
ENVIRONMENTAL PARAMETERS OBSERVED IN THE MAUI REGION, MARCH 1981

ARL:UT
BS-83-1159
ACK - GA
10 - 25 - 83

It is to be noted that after the sharp drop in levels at 0800 on 17 October, the high frequency spectral levels in both the wave and microseism spectra remain essentially constant throughout most of the day. It is believed that this lower level of activity is associated with nonlinear wave-wave interactions involved in the maintenance of the spectral form of the southeasterly sea, as discussed, for example, by Hasselmann.[24] In this regard, we note further that, in this time interval, the wave and seismic spectral levels about the peak remain roughly constant. Further, initially the wave peak simply decays in amplitude and shifts little in frequency, and only with further wave field decay does the peak shift to higher frequencies. This behavior is mirrored in the microseism response (also see Fig. 4). Moreover, as discussed above, it is observed that the narrower the spectra, the closer is the frequency relationship to 2:1. This has been noted often in this study, the peak frequency of the seismic spectrum generally exceeding twice that of the wave spectrum during the early development of the wave field. On the other hand, the development of the wave spectrum usually lags on the seismic field under a changing wind regime. It is now clearer why the seismic spectrum (and general wind induced ambient noise field) correlates more closely with the wind than with sea state. Correlation with sea state occurs under steady state conditions.

This overall behavior leads us to conclude that the nonlinear resonant interactions held to be responsible for cross-spectral energy transfer and the preservation of the shape of the wave spectrum of the changing sea are also a significant source of microseism generation. We have found the levels of this activity to be typically of the order 10^{-11} m^2/Hz, and the power ratio of the spectral peaks to be around 10 $(microns/meter)^2$. Both values are an order of magnitude less than those associated with the more energetic processes invoked when two distinct wave fields are in opposition. This activity is no doubt present all the time when the winds are active, but is swamped when opposing seas are interacting.

2. Event 21-25 October 1981

The sequence of 21-25 October, also shown in Fig. 4, can reviewed briefly by way of comparison.

Throughout 21-23 October, a local sea develops in the Maui region, under the influence of increasing northerly winds. By 23 October, the significant wave height has risen to just less than 3 m. Microseism activity develops with the wave field and, by early on 23 October, the spectral peaks are close to a 2:1 frequency relationship. In line with the reasoning outlined above, the generation mechanism at this time is attributed to wave-wave interactions associated with the developing sea.

At around noon on 23 October, another southeasterly event occurs in Cook Strait. The wind swings quickly from the north to southeast and increases to over 30 m/sec before falling over the next 24 h. While the wave and seismic response is compounded by another change in the wind field on 25 October, the same general behavior as was observed in the earlier event can be recognized. Once again, the new southeast wave field develops quickly. The peak frequency falls below 0.1 Hz and masks the ever present southwesterly swell, and the frequency relationship steadily approaches a value of 2:1 (also see Fig. 7).

As in the earlier event, two distinct periods can be identified in the microseismic response. Activity reaches high levels (approximately 10^{-9} m^2/Hz) while the two opposing seas are interacting, although the peak activity is less than that recorded during the event of 17 October, in spite of the fact that the wind speed is a little higher. It is believed this is due to the fact that the shift in wind bearing is only around 100^{o} and the seas are thus not directly opposed, rather than there being any saturation effect. Further, the microseism activity drops to lower levels as before, presumably when the original wave field has been suppressed. The dominant source of the microseisms again then becomes the wave-wave interactions associated with the adjustment of the dominant wave field.

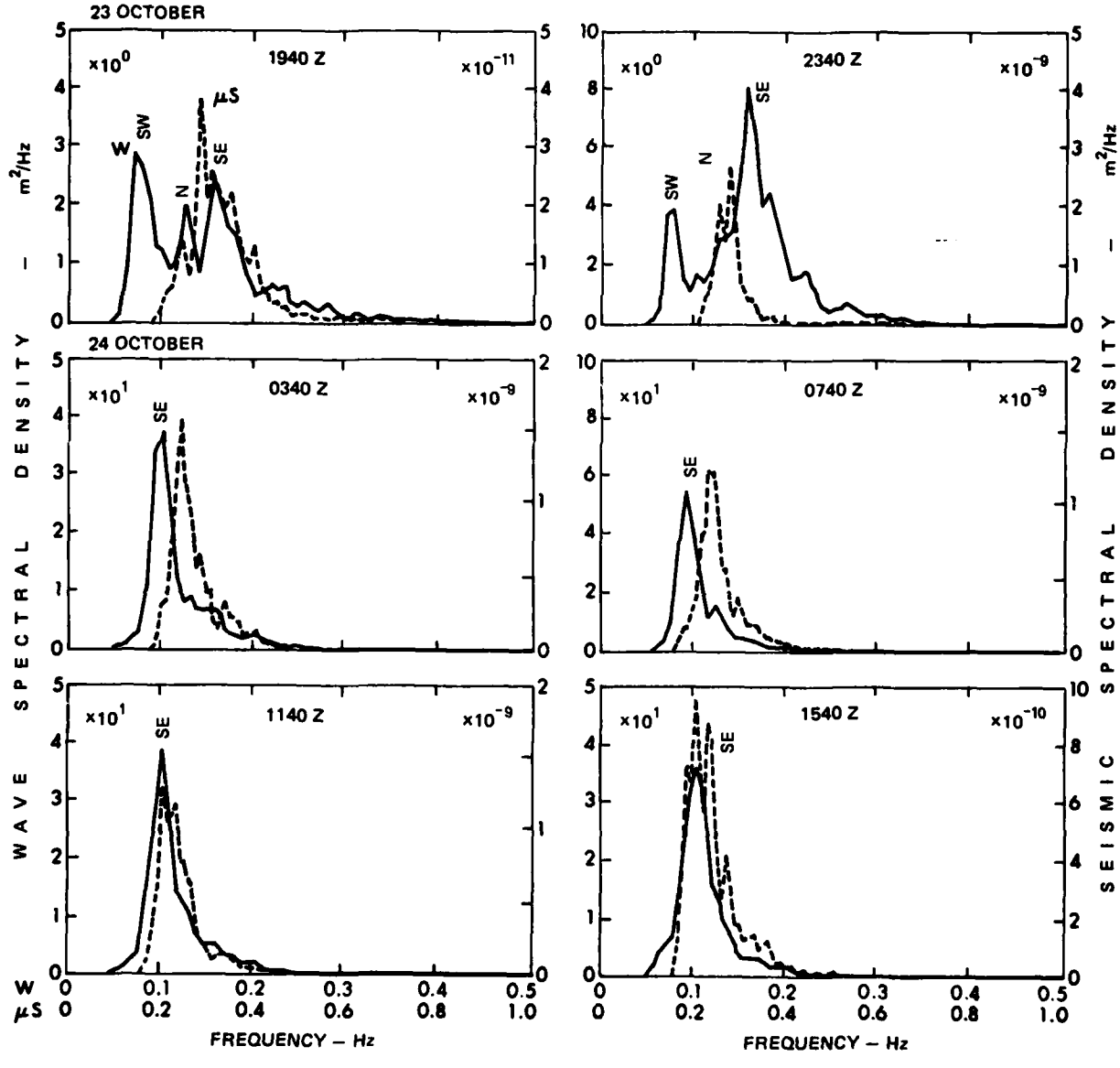

FIGURE 7
FOUR – HOURLY SPECTRA FOR THE EVENT ON 23 OCTOBER 1981

ARL:UT
AS-83-1146
ACK - GA
10 - 25 - 83

In the next sections, supplementary evidence is presented in support of the general conclusions outlined above.

VI. SPECTRAL OVERLAP AND WAVE-WAVE INTERACTIONS OF OPPOSING SEAS

In most of the southeasterly events, the switch in wind direction, increase in wind speed, and growth of the southeasterly sea takes place so rapidly that the four-hourly recordings on which the routine sampling was based rarely allowed the detail of the spectral development and decay to be resolved. The events of October 1981, analyzed above, were typical in this regard (see Fig. 7). Between 2340Z on 23 October and 0340Z on 24 October, the southeasterly sea developed rapidly and all evidence of the original northerly sea and southwesterly swell was lost in the wave spectra.

In an event on 28-29 March 1981, however, the wind changes took place sufficiently slowly for the essential features of the development to be resolved (see Figs. 6 and 8). For several days prior to 28 March, the winds in the Maui region were from the north-northwest and fairly steady around 10 m/sec. On 27 March the wind increased briefly to a speed in excess of 15 m/sec, decayed to zero, changed bearing to the southeast (a change of around 180^0), and increased to over 20 m/sec in a period of about 20 h.

The combination of the 180^0 bearing shift and high wind speeds before and after the change accounts for the large seismic response observed at that time. The significant wave height prior to the wind shift was 4 m, compared with 3 m at the period of maximum wind speed on 28 March. Microseismic activity reached a peak just after the wind change, but before the winds reached their new maximum of 20 m/sec. The equivalent seismic significant wave height reached a value of 25×10^{-6} m (maximum power spectrum level of around 4×10^{-10} m^2/Hz) and the peak spectral power ratio approached 50 $(micron/meter)^2$. The period ratio remained in excess of 2 from early on 27 March until the seismic activity decreased on 28 March.

An examination of the spectral development for 28-29 March, shown in Fig. 8, is instructive. The spectra for 28 March show the growth of the

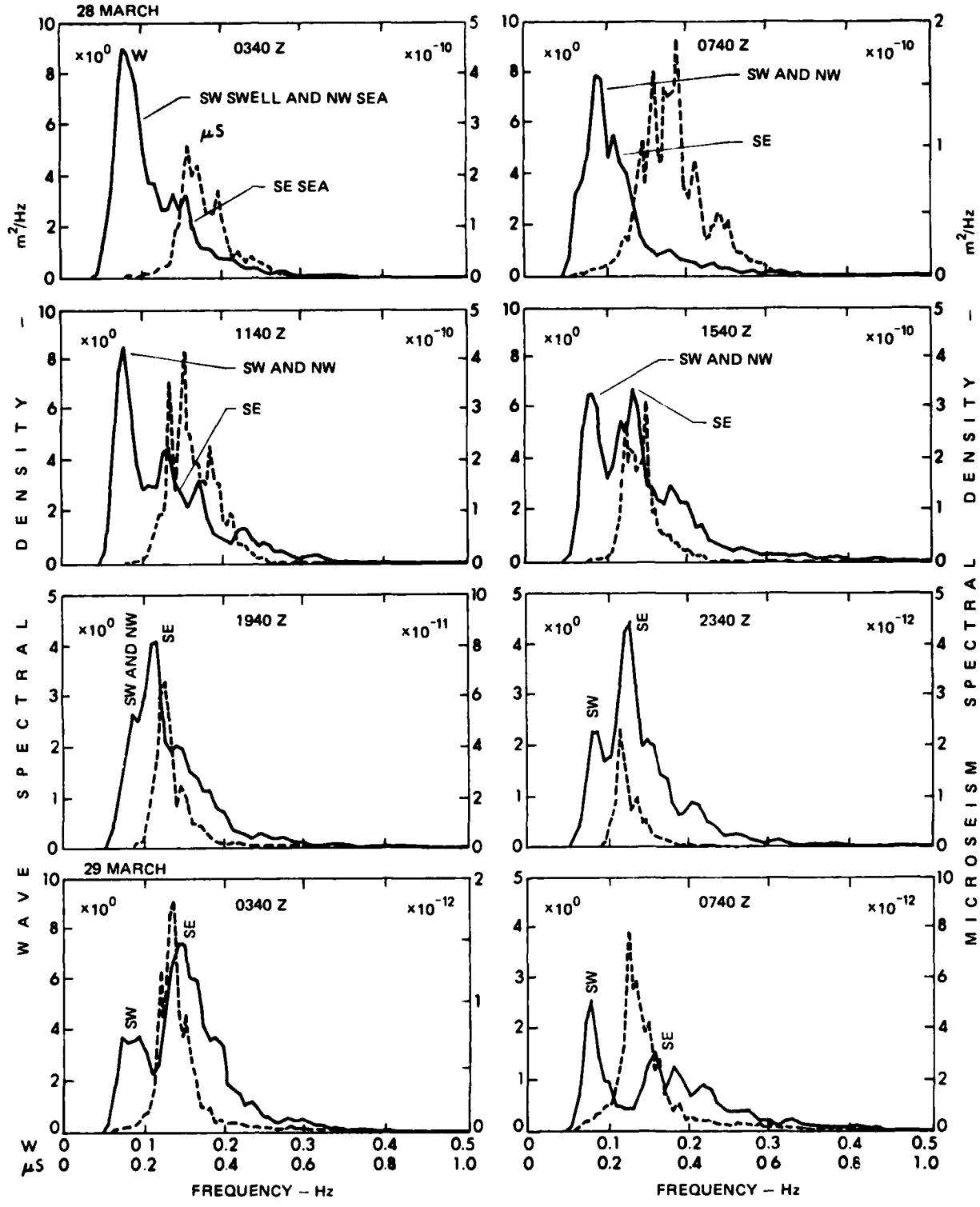

FIGURE 8
FOUR – HOURLY SPECTRA FOR THE PERIOD 28-29 MARCH 1981

ARL:UT
AS-83-1147
ACK - GA
10 - 25 - 83

southeasterly sea relative to the energy peak comprising a southwesterly swell and the original sea from the northwest. At 1540Z, the levels are comparable, the two spectra are conveniently resolvable, and the region of overlap can be identified.

An examination of the spectra shows that the seismic activity again occurs essentially in the region of overlap. On the linear presentation used, there is no seismic energy apparent corresponding to the wave energy associated with the southwest swell and the northwest sea. Whatever is present is swamped by the intense activity associated with the frequency region in which the two opposing local sea spectra overlap.

On the basis of theory (see Eq. (4)), the seismic activity resulting from the wave-wave interactions should be proportional to the product of the power spectra of the two seas. Assuming an ω^{-5} frequency dependence for the high frequency tail of the northwest component, a reasonable qualitative evaluation of the spectra of the two opposing wave trains is possible. Following this procedure and establishing the product of the two resolved spectra leads to a spectral shape for the microseism signal comparable with that actually observed (see Fig. 9). It seems clear that the dominant seismic signal is generated by the interaction of the two wave trains.

In the subsequent 24 h, the seismic spectral form reflects the degree of spectral overlap of the two opposing wave fields, although in some cases this is obscured by either the plotting gains used or extraneous wave energy arriving from distant fetches to the southwest.

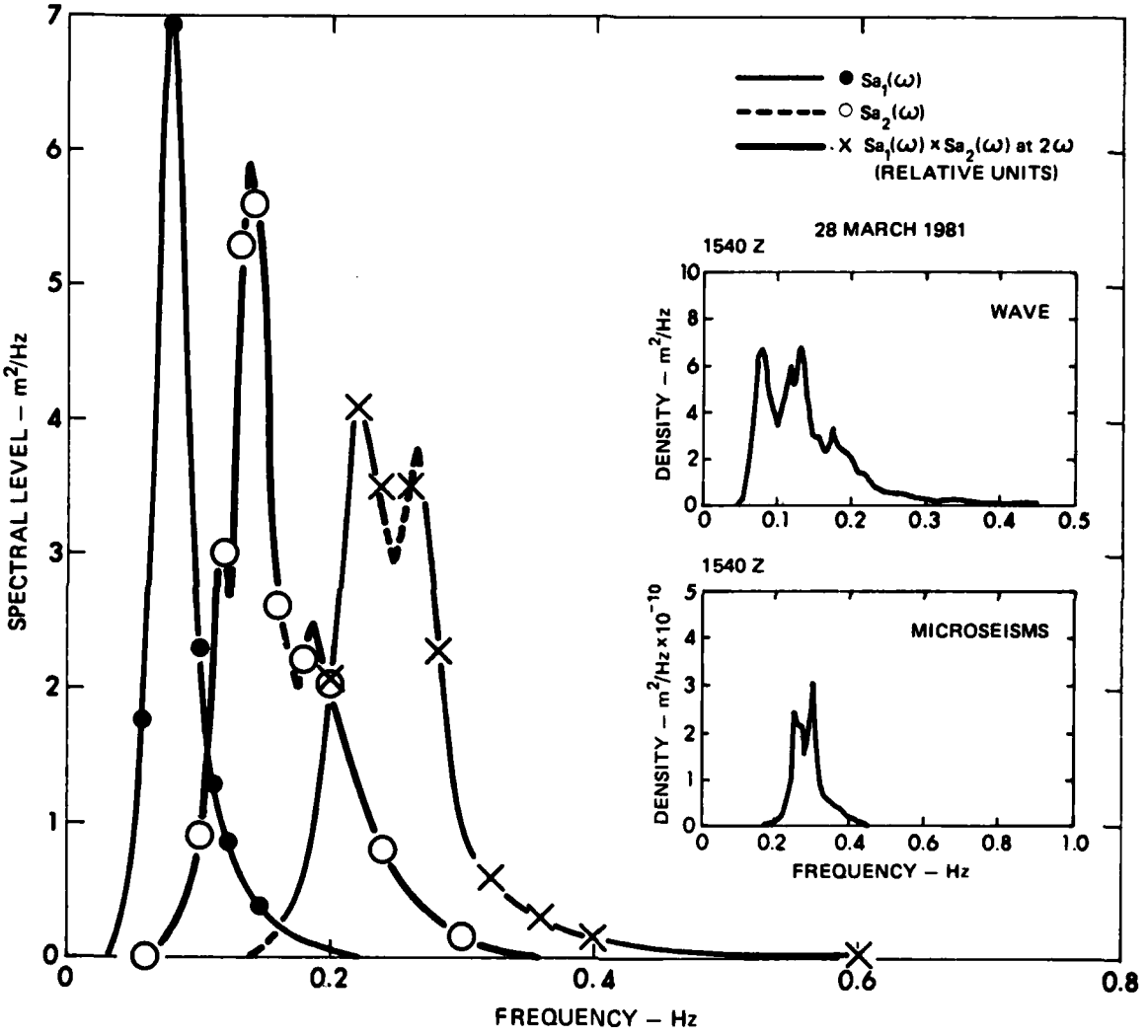

FIGURE 9
MICROSEISM GENERATION BY TWO OPPOSING WAVE FIELDS

ARL:UT
AS-83-957
ACK - GA
10 - 5 - 83

VII. THE DEPENDENCE OF SEISMIC RESPONSE ON SEA STATE/WIND SPEED

According to theory (Eq. (4)), there should be a square law relation between two corresponding spectral levels when appropriate account is taken of the frequency term in the expression. However, while an inspection of the experimental data clearly indicates some power law dependence between the seismic response and the ocean wave field, complexities in the latter and distortions arising when the frequency relationship between the two fields was not exactly 2:1 obscured an examination based on spectral levels. It proved more informative to consider the significant heights (or variances) using the connection between the two provided by Longuet-Higgins' original formalism.[9]

A plot of the logarithm of the microseism significant height (or variance) multiplied by $\bar{T}^2$, where $\bar{T}$ is the mean ocean wave period, against the logarithm of the ocean wave significant height (or variance) for all the Maui spectral data for the two years (1980 and 1981) is given in Fig. 10. A least square regression fit establishes the slope as 2.06, with a correlation coefficient of 0.81, and apparently confirms the square law expected.

In an alternative evaluation, the data from the major southeasterly events recorded in 1981 were grouped according to the two wind directions, SE and W, and a similar relationship established (Fig. 11). In this case, however, a possible threshold level appears, below which the wind induced component of the microseism activity is not truly manifest. The grouping for the two data sets implies moreover that, even though a square law dependence still prevails, the microseism response is less energetic for the westerly winds.

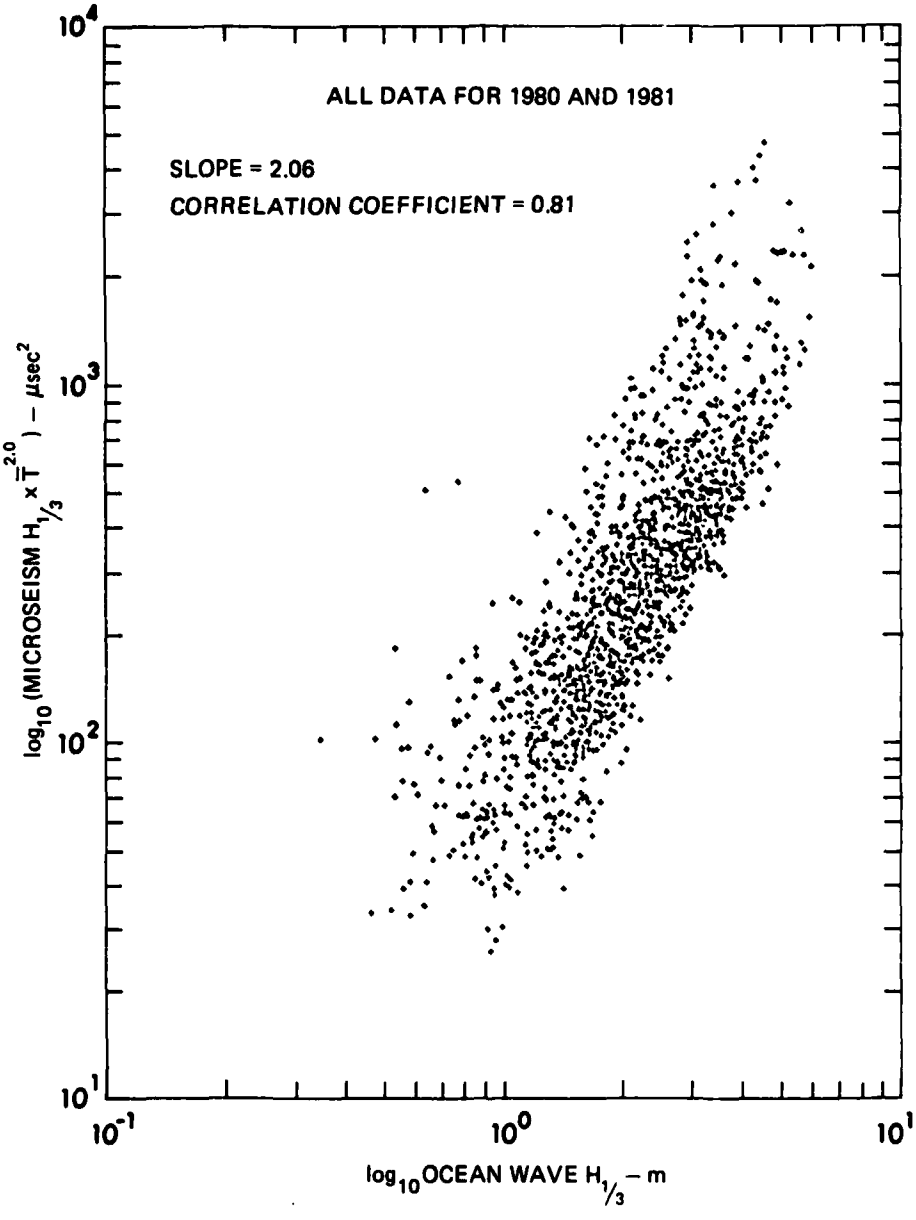

FIGURE 10
RELATIONSHIP BETWEEN SIGNIFICANT HEIGHTS
$\bar{T}$ IS OCEAN WAVE MEAN PERIOD

ARL:UT
AS-83-1148
ACK - GA
10 - 25 - 83

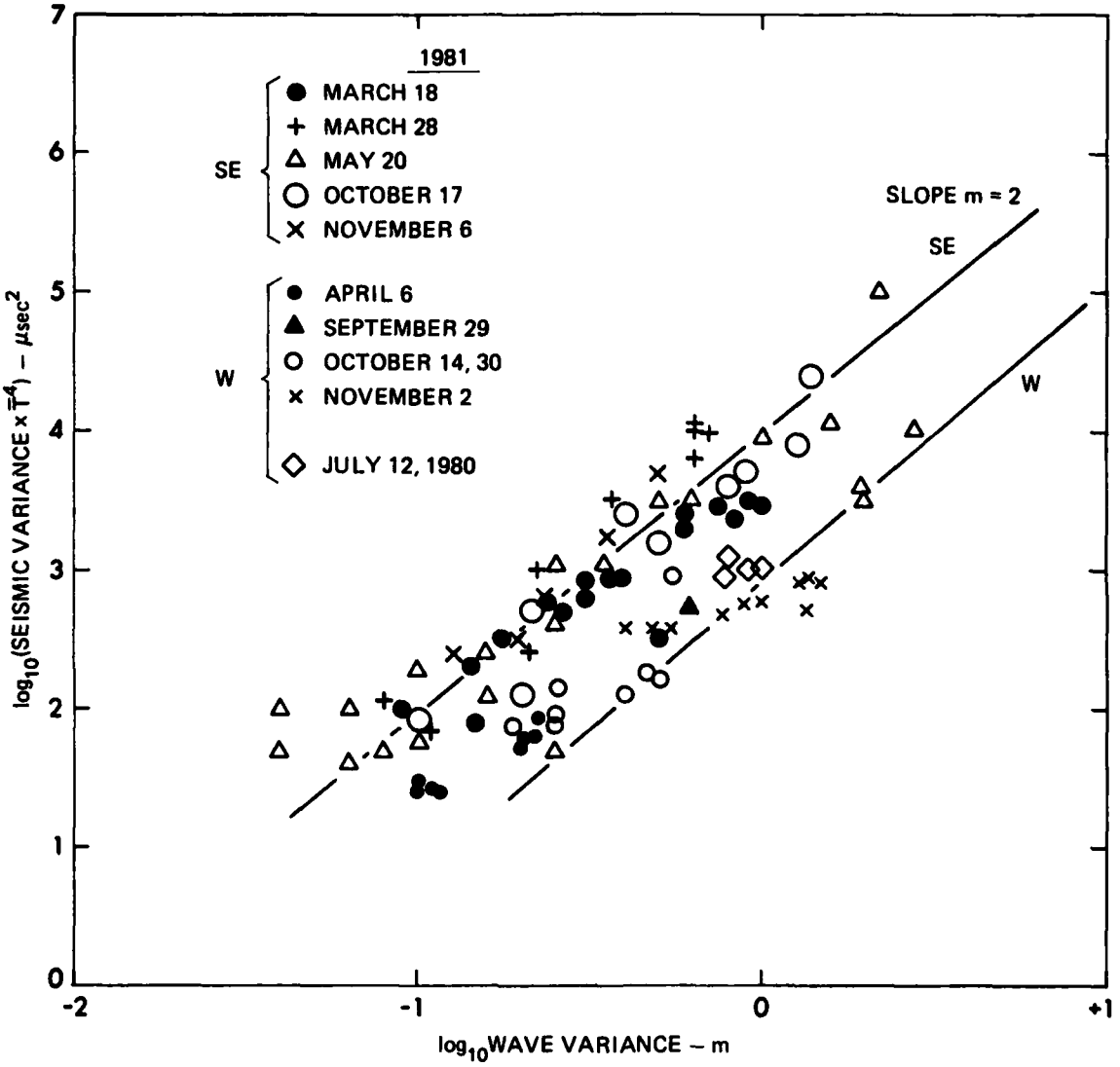

FIGURE 11
RELATIONSHIP BETWEEN SEISMIC AND WAVE VARIANCES OF SPECTRA GROUPED ACCORDING TO WIND DIRECTION

ARL:UT
AS-83-1149
ACK - GA
10 - 25 - 83

VIII. SPECTRAL SLOPE DEPENDENCE

Another test of the interpretation that wave-wave interactions are responsible for the microseism activity observed in the cases reported involves the frequency dependence of the ratio $Su(2\omega)/[Sa(\omega)]^2$ (see Eq. (4)). This can be tested by plotting the logarithm of this ratio against the logarithm of the frequency. Alternatively, one can establish the dependence of the ratio on frequency by measuring the spectral slopes of the two spectra in the frequency range of interest, which is normally above the frequency of the spectral maximum f_m. While both procedures are applicable, lack of a precise 2:1 frequency relationship in some spectra can distort the ratio determined. Furthermore, whichever approach is followed, difficulties can also arise when the wave field is complicated by the presence of components from wave fields other than those of interest.

In general, it has proven easier to examine this question through the measurement of the high frequency spectral slopes using the logarithmic plots of the two spectra, rather than the linear equivalent represented earlier. The linear plots are more helpful in establishing initial correlations and what is occurring within the wave field; but, for spectral slope evaluations, the greater dynamic coverage provided by the logarithmic plots is desirable. Typical logarithmic plots of the four-hourly spectra for 17-19 March 1981 are shown in Figs. 12-14.

To establish spectral slopes, one should strictly take account of the exponential terms in the expressions for the Pierson-Moskowitz (PM) or JONSWAP spectra.[29,32] However, well above f_m the correction involved is not significant. Accordingly, the spectral slopes were established initially from a plot of $\log_{10} Sa(f)$ (and $Su(2f)$) against $\log_{10}(f)$.

Using data for 16 October as an example, the slopes of $Sa(f)$ and $Su(2f)$ above f_m are established as -4.5 in both cases. This leads to a frequency dependence for the slope ratio $R_s=Su(2f)/[Sa(f)]^2$ of +4.5, which can be compared with the value +4 required by the theory of wave-wave interactions (Eq. (4)). Evaluations of many spectral pairs, however,

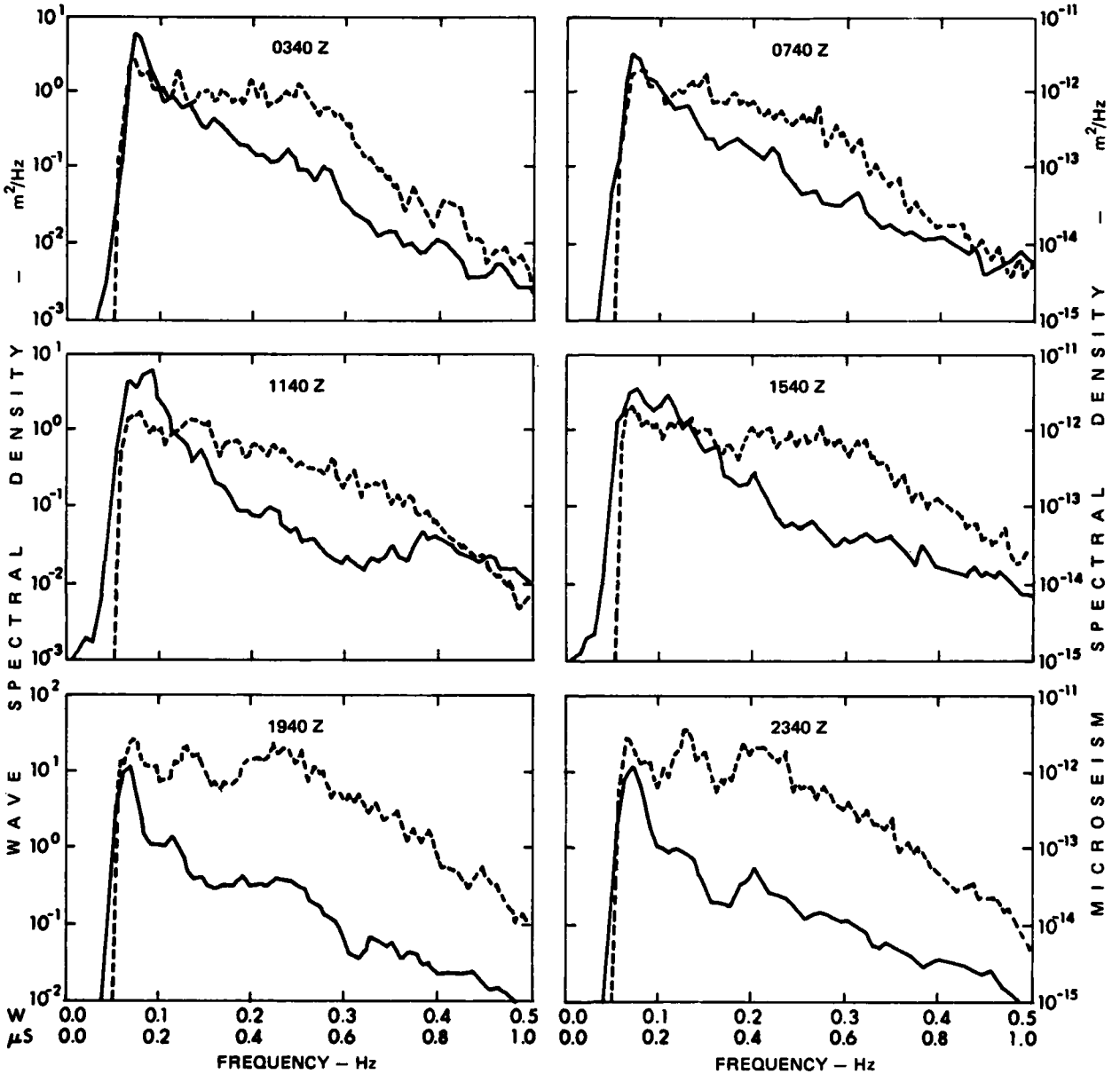

FIGURE 12
LOGARITHMIC SPECTRA FOR 17 MARCH 1981

ARL:UT
AS-83-1150
ACK - GA
10 - 25 - 83

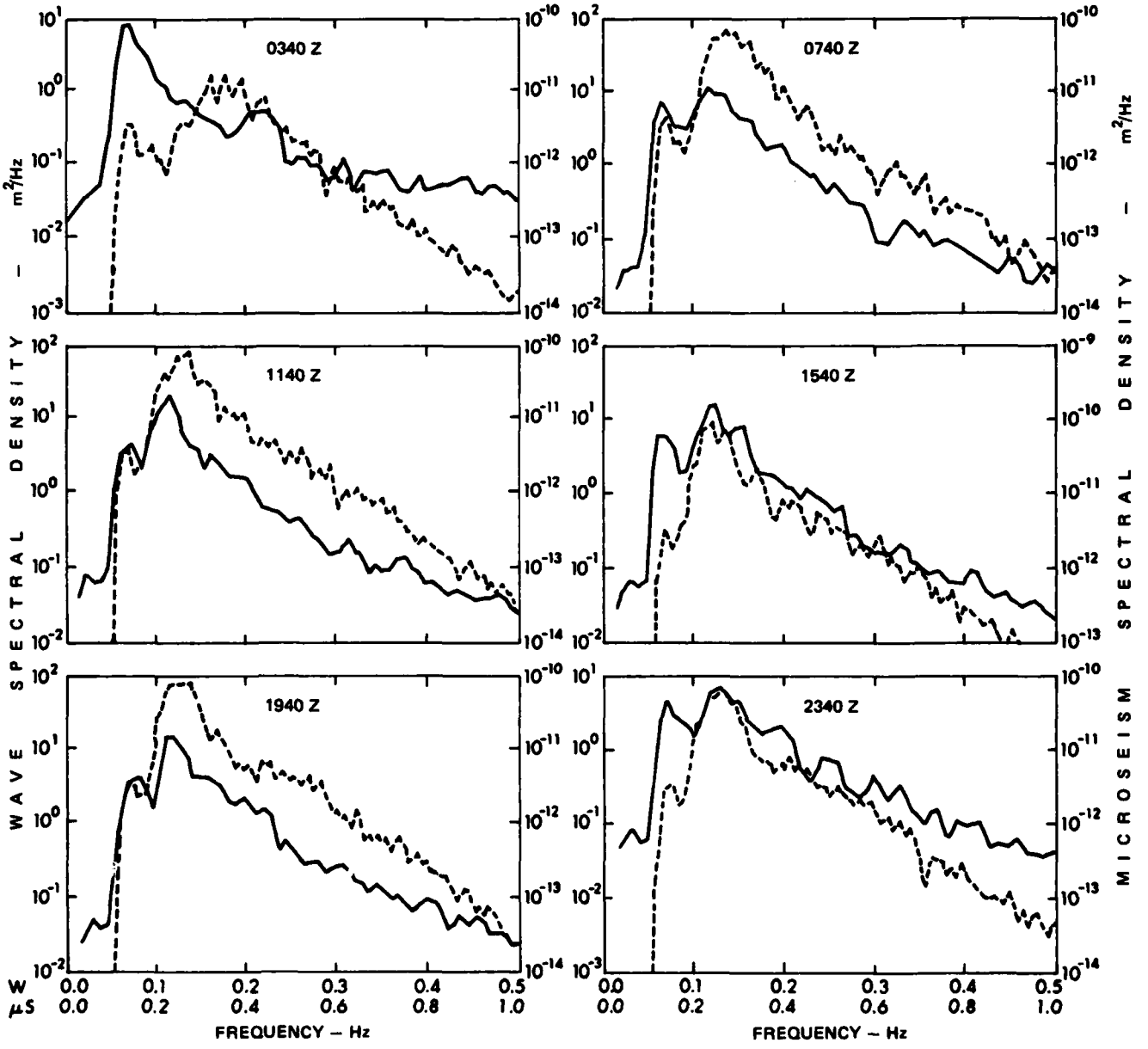

FIGURE 13
LOGARITHMIC SPECTRA FOR 18 MARCH 1981

ARL:UT
AS-83-1151
ACK-GA
10-25-83

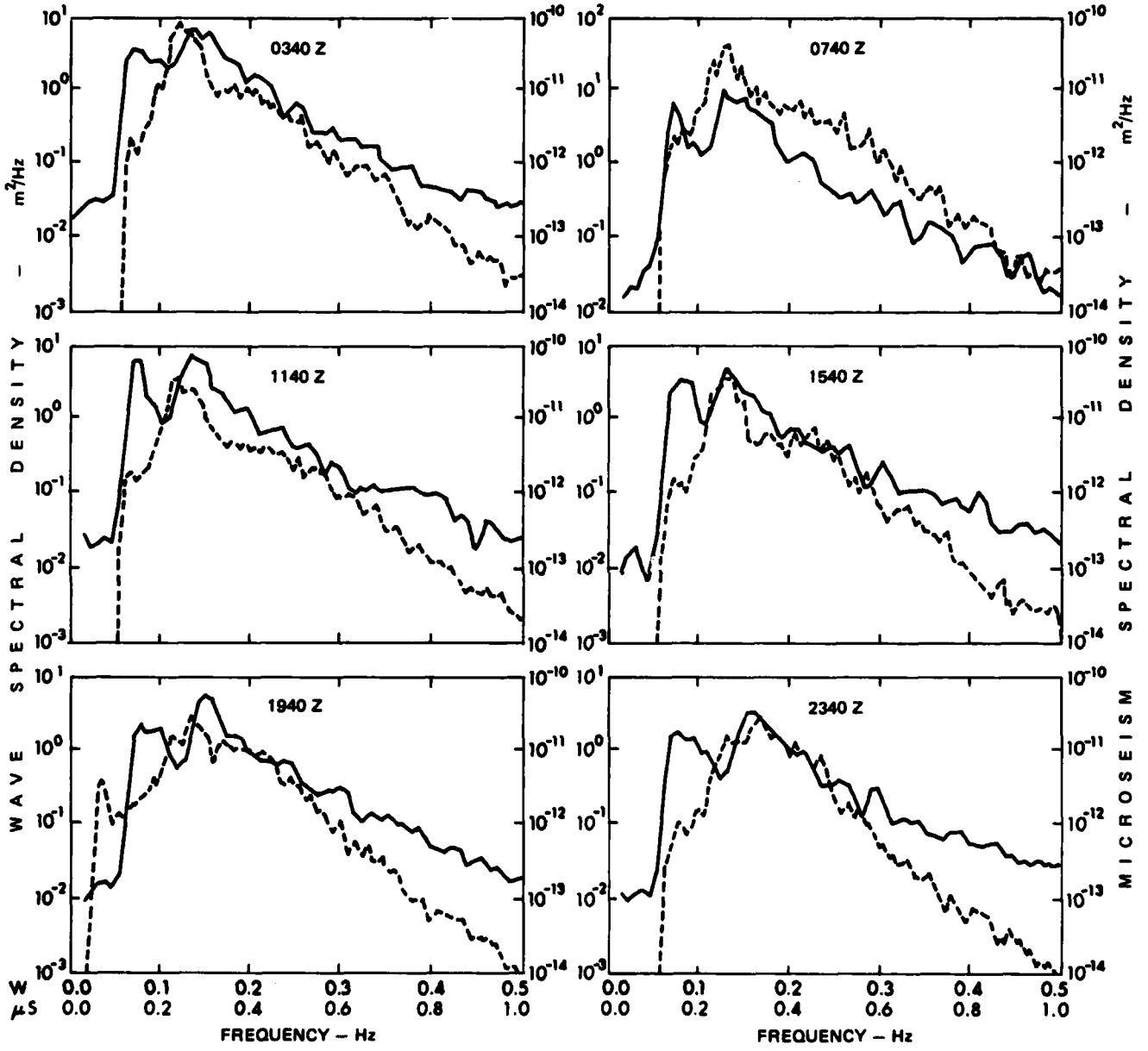

FIGURE 14
LOGARITHMIC SPECTRA FOR 19 MARCH 1981

ARL:UT
AS-83-1152
ACK - GA
10 - 25 - 83

showed that, while most values of R_s lay between 3 and 4, values ranged from 1 to 9.

To establish some meaningful average for all conditions, an approach based on nondimensionalized spectra was followed. This approach had been applied successfully to the wave spectra to establish properties of the wave field and it was extended to the microseismic spectra. For details, the reader is referred elsewhere,[30] but essentially a nondimensionalizing procedure based on that of Hidy and Plate[33] was used. As Liu[34] had found this scheme to give a universal function for steady, growing, and decaying wave conditions, it was considered appropriate to apply the nondimensionalization in the present case to spectra of southeasterly seas, grouped according to these same classifications.

The southeast spectra were initially selected from the total set (about 5000 spectra) using the constraints that the wind had been continuously in the southeast quarter for at least 6 h prior to the wave recording and that the spectrum contained at least 33 degrees of freedom. Each of the spectra so selected was then considered along with the wind records to ensure that a southeasterly wave component could clearly be identified. Ambiguous spectra were again discarded, as were any containing significant swell, and finally only 349 southeasterly spectra were selected for processing from the total set. The criteria applied to further subdivide this group were:

GROWING Spectra, G_f:

I. Wind speeds increasing
II. Ocean wave spectral peak migrating to lower frequencies and increasing in amplitude

GROWING PEAK Spectra, G_p:

I. Wind speeds increasing
II. Ocean wave spectral peak increasing in amplitude

STEADY Spectra, S:

I. Wind speeds steady to within 1 m/sec for at least 4 h
II. Local southeast spectral peak steady in both amplitude and frequency

DECAYING Spectra, D_f:

I. Wind speeds decreasing
II. Wave spectral peak migrating to higher frequencies and decaying in amplitude

DECAYING PEAK Spectra, D_p:

I. Wind speeds decreasing
II. Wave spectral peak decaying in amplitude

The nondimensionalization involves multiplying the variance spectral density function by the peak frequency f_m, and dividing by the variance σ^2. Each spectrum in a particular group was nondimensionalized in this way and the group then averaged to arrive at the universal spectral function $\psi(f/f_m)$ for the group. This average spectrum was then curve fitted with the normalized JONSWAP function[30,32] to give a new function $\tilde{S}(\tilde{f})$. Various parameters were derived from this best fit curve for other studies. For the present analysis, measurements of the spectral slope were made for various intervals at frequencies above f_m by performing a linear regression analysis on log $\tilde{S}(\tilde{f})$ as a function of log $\tilde{f}$. These intervals were selected by a visual inspection of the normalized spectra. As an example, the nondimensional spectra for the S-group (SE winds) are given in Fig. 15 and the results of the analysis in Table I.

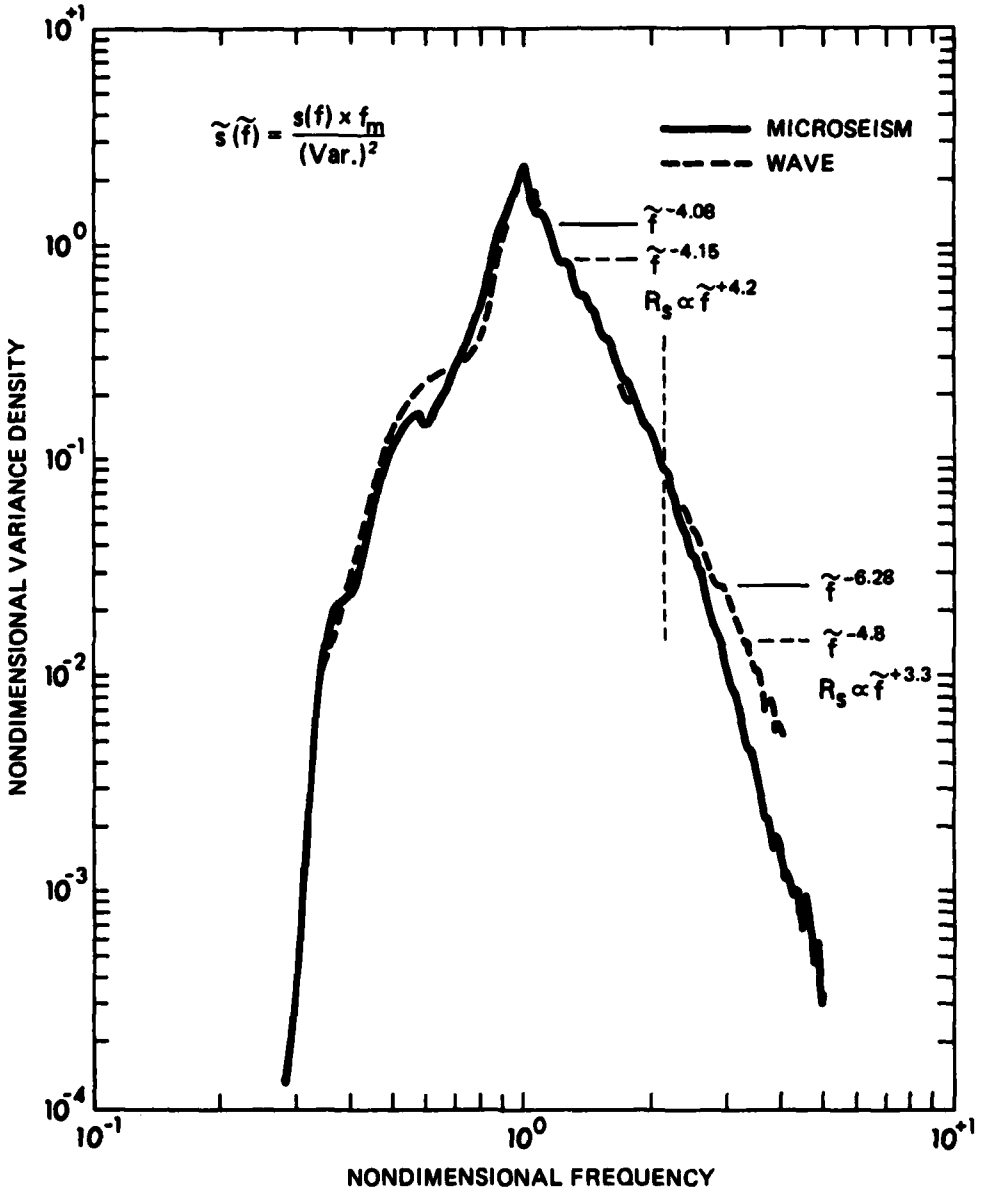

FIGURE 15
NONDIMENSIONAL SPECTRAL FUNCTIONS FOR THE S-GROUP

ARL:UT
AS-83-1139
ACK - GA
10 - 25 - 83

TABLE I

VALUES OF THE RATIO $Su(2\omega)/[Sa(\omega)]^2$
EVALUATED FROM THE SPECTRAL SLOPES OF THE NONDIMENSIONAL SPECTRA

SE SPECTRUM GROUP	SPECTRAL SLOPES AND SLOPE RATIO: WAVE FREQUENCY RANGE 1.1-3.0	WAVE FREQUENCY RANGE 3.0-4.5	WAVE FREQUENCY RANGE 1.1-4.5	MICROSEISM FREQUENCY RANGE 1.1-2.0	MICROSEISM FREQUENCY RANGE 3.0-4.5	MICROSEISM FREQUENCY RANGE 1.1-4.5	$R = Su(2\omega)/[Sa(\omega)]^2$ FREQUENCY RANGE (xf_m) 1.1-2.0	$R = Su(2\omega)/[Sa(\omega)]^2$ FREQUENCY RANGE (xf_m) 3.0-4.5	$R = Su(2\omega)/[Sa(\omega)]^2$ FREQUENCY RANGE (xf_m) 1.1-4.5
STEADY (S)	-4.15 ±0.05	-4.8 ±0.08	-4.53 ±0.001	-4.08 ±0.05	-6.28 ±0.09	-6.01 ±0.05	+4.2	+3.3	+3.0
GROWING PEAK (G_p)	-4.6 ±0.1	-5.4 ±0.2	-4.9 ±0.007	-5.58 ---	-5.58 ---	-5.58 ±0.04	+3.6	+5.2	+4.2
GROWING ($G+G_f$)	-4.43 ±0.09	-4.6 ±0.3	-4.44 ±0.007	-6.52 ---	-6.52 ---	-6.52 ±0.03	+2.3	+2.7	+2.3
DECAYING PEAK (D_p)	-3.9 ±0.1	-6.2 ±0.2	-4.62 ±0.008	-4.08 ±0.07	-6.8 ±0.1	-5.46 ±0.1	+3.8	+5.6	+3.7
STEADY SOUTHWEST			-4.5			-4.86			+4.1

The first feature apparent in the processed spectra is that for local seas both the ocean wave and seismic spectra are apparently well described by a universal function under the Hidy and Plate nondimensionalization. Moreover, the spectra for decaying, growing, and steady conditions are all found to be similar under this nondimensionalization. This implies that the wave field itself rather than the atmospheric input is responsible for preserving the similarity of the ocean wave spectra, a fact relevant to the role of nonlinear wave-wave interactions in the process.

The second feature apparent in Table I and Fig. 15 is that the universal functions for the wave spectra suggest the existence of a double equilibrium range, with slope values roughly the same in all groups. For f/f_m in the range 1.1 to 3, the spectrum level dependence on frequency is about f^{-4}, while above $f/f_m=3$ the proportionality is closer to f^{-5}. This result, which has its parallel in work by Forristal,[35] is discussed further by Ewans.[30] In the present context, this property of the spectra was recognized in evaluating the slope of the spectral curves above f_m. The measured values and the resultant values of R_s for each spectral group (except D_f) are tabulated in Table I. In all cases, the correlation coefficient for the regression analysis was greater than 0.9.

The S-group contains the most spectra (39) and is considered to provide the most reliable spectral parameters. An examination of Table I shows that, in the region closest to the peak frequency, the value of R_s is close to +4. In this same frequency interval, the value for G_p and D_p groups is also close to +4, the average for all three being +3.9. In the other spectral ranges, there is more variation in R_s, but average values for these three groups in the frequency intervals 3.0-4.5 Hz and 1.1-4.5 Hz at +4.4 and +3.6, respectively, are still close to the theoretical value.

The values of R_s for the G_f and D_f (not shown in Table I) groups are lower in all three frequency intervals. The number of spectra involved is small in each case, but the anomaly is perhaps not surprising when there is movement in the spectral peak.

Also shown in Table I are the spectral slopes for a steady SW sea and once again we find a value of R_s close to +4. The evidence from R_s therefore appears to support the thesis that nonlinear interactions within the wave field are the source of the microseisms observed.

Anomalously low values of R_s were also observed in the case of two opposing wave fields and this needs further comment.

As has been outlined above, the most energetic seismic activity experienced in this program occurred when a wind change of 180^0 brought two opposing seas into interaction. This activity was confined to the region of spectral overlap. It initially grew quickly to high levels over a wide frequency band but died equally quickly to a lower level once the new wave field became dominant (see Fig. 4, for example).

A study of the slopes of individual spectra throughout such an event shows that the low values of R_s result because of high negative slope values in the seismic spectra (see Table II and Fig. 4). However, the seismic slope decreases quickly after the peak activity and falls to "normal" values of the order -6. It is believed that at this time the original wave field has been effectively wiped out and that the residual seismic activity then results from wave-wave interactions within the single wave field.

It is interesting to speculate whether the very high levels of seismic activity arise through standing wave effects of the type originally conceived by Longuet-Higgins[9] or more energetic nonlinear interactions involving the two wave fields. The highest levels recorded, of the order 10^{-9} m^2/Hz, are 10 to 100 times greater than the values observed when activity is associated with a single wave field. The nonlinear processes require oppositely traveling components, and evidence from several sources confirm these do exist in a single sea. For instance, Tyler et al.[36] quote radio measurements which give an upper limit of 0.02 for the upwind/downwind ratio in wave energy flux. One may therefore expect the seismic response from the interaction of two opposing wave fields of

TABLE II

VARIATION OF SPECTRAL SLOPE
THROUGHOUT THE EVENT 16-19 OCTOBER 1981

	TIME	WAVE SPECTRA				MICROSEISM SPECTRA			
DATE	(Z)	FREQ.RANGE	SLOPE	ERROR	C.COEFF.	FREQ.RANGE	SLOPE	ERROR	C.COEFF.
October 16	0740	0.15-0.5	-4.29	0.13	0.98	0.3-1.0	-5.92	0.18	0.98
	2340	0.15-0.5	-4.15	0.10	0.98	0.3-1.0	-9.06	0.09	0.99
October 17	0340	0.15-0.5	---	---	---	0.3-1.0	-7.94	0.12	0.99
	0740	0.10-0.5	-4.62	0.07	0.99	0.3-1.0	-6.23	0.22	0.97
	1540	0.10-0.5	-4.56	0.09	0.99	0.3-1.0	-5.16	0.11	0.98
October 18	0740	0.15-0.5	-4.42	0.15	0.98	0.25-1.0	-5.24	0.11	0.98
	2340	0.15-0.5	-4.02	0.13	0.98	0.30-1.0	-5.8	0.18	0.98
October 19	2340	0.20-0.5	-4.09	0.2	0.97	0.40-1.0	-5.12	0.22	0.97

roughly equal magnitude to be some 100 times greater than that from a single wave field alone. The observed ratio may therefore be significant and lead to the conclusion that nonlinear interactions are responsible for microseism generation in both single and opposing seas.

The lower values of R_s for opposing seas are nevertheless still intriguing in view of the ω^2 dependence predicted in some theoretical analyses,[11] but we must conclude that the spectral slope ratios are not helpful in resolving this question. The relative distortions in wave and microseism spectra make it difficult to draw any definite conclusions. However, overall the evidence from the spectral ratios supports the role of nonlinear interactions in the seismic effects observed.

IX. AMBIENT NOISE CHARACTERISTICS

A. Spectral Behavior with Wind Speed

Because the geophysical data required to effectively evaluate the properties of the transfer function in Eq. (3) are not available, we can as a first approximation assume with Urick[23] that the sea bottom is an infinite surface, radiating and responding to plane waves incident from above or below, and use the observed microseism levels to establish the associated pressure field and compare the results with other ambient noise measurements.

The results for the event of 16-20 October (see Fig. 4) are shown in Fig. 16. Included for comparison is a spectrum taken on 24 October during the period of high activity later in the month. In this and subsequent figures, spectrum levels are related to a 1 Hz bandwidth and derived from the equivalent form of Eq. (2), with f expressed in hertz:

$$Sp(2f) = 2\pi^3 \frac{\rho^2 g^2}{c^2} f^3 \left[Sa(f)\right]^2 \quad . \tag{6}$$

Figure 16 demonstrates very well the nature of the spectral development in an event of this kind. At 0340Z on 17 October, the wave and seismic levels are high. As the wind drops, the spectral peak initially decreases in magnitude without shifting significantly in frequency, but evidence of movement in the peak is apparent by 1940Z on 18 October. Thereafter, the peak continues to decrease and shift to higher frequencies.

By 1940Z on 19 October, the seismic activity associated with the ever-present low frequency wave energy becomes visible. This component of the wave field has its origin primarily in distant southwesterly swells from the Southern Ocean,[27,28] but energy will also be present from distant fetches throughout the Tasman Sea.

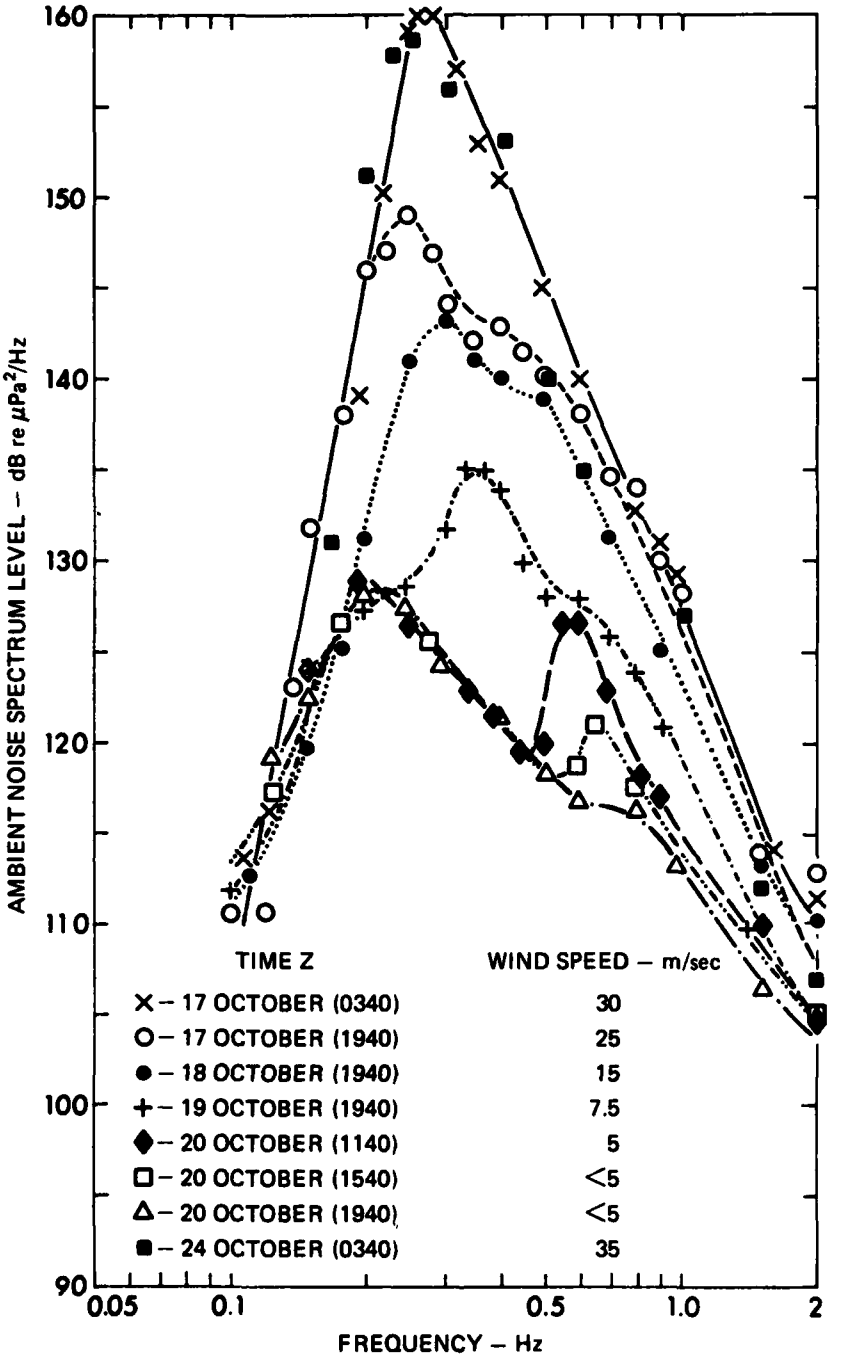

FIGURE 16
DERIVED AMBIENT NOISE LEVELS FOR VARIOUS WIND SPEEDS

ARL:UT
AS-83-1153
ACK - GA
10 - 25 - 83

As the local sea continues to decay, the low frequency energy becomes more and more dominant. In the Maui region, wave and seismic activity rarely drop below the level represented by the spectrum of 1940Z on 20 October ($H_{1/3} \approx 1.2$ m). The statistics of five years indeed show that the average significant wave height is 2-3 m.[27] This background will therefore generally obscure wind dependent effects at low wind speeds. Background levels are much lower on the east coast of New Zealand,[30] but high residual swell levels can be expected in most open ocean areas.

It is not clear from the evidence whether the seismic activity associated with this low frequency wave energy is the result of nonlinear interactions between spectral components from distinct fetches or coastal reflection processes in which incident swell interacts with its own reflected energy.

B. Comparison with Other Data

The ambient noise levels of Fig. 14 are compared with other ambient noise data in Fig. 17. The data selected for comparison are those considered to be most relevant on the basis of the review carried out by Nichols.[17]

Within the bandwidth 0.1-2 Hz, the Tapley and Worley and the Eleuthera data fall convincingly within the range of the New Zealand spectra. Further, the wind dependence is of the same form. However, the rise in spectral level below 0.1 Hz is not observed in the seismic results for which a low frequency plotting limit of 0.09 Hz was imposed. Above 2 Hz, the seismic data were affected by unrelated effects and are not included, but it is clear that the trends above 2 Hz are comparable in all cases.

The Perrone and Bermuda data do not conform so well, but the authors acknowledge uncertainties in the recording system below 1.0 Hz.

Results from the east coast of New Zealand, where residual wave and seismic levels are lower and hydrophone information is also available, are being processed and will be reported in due course.

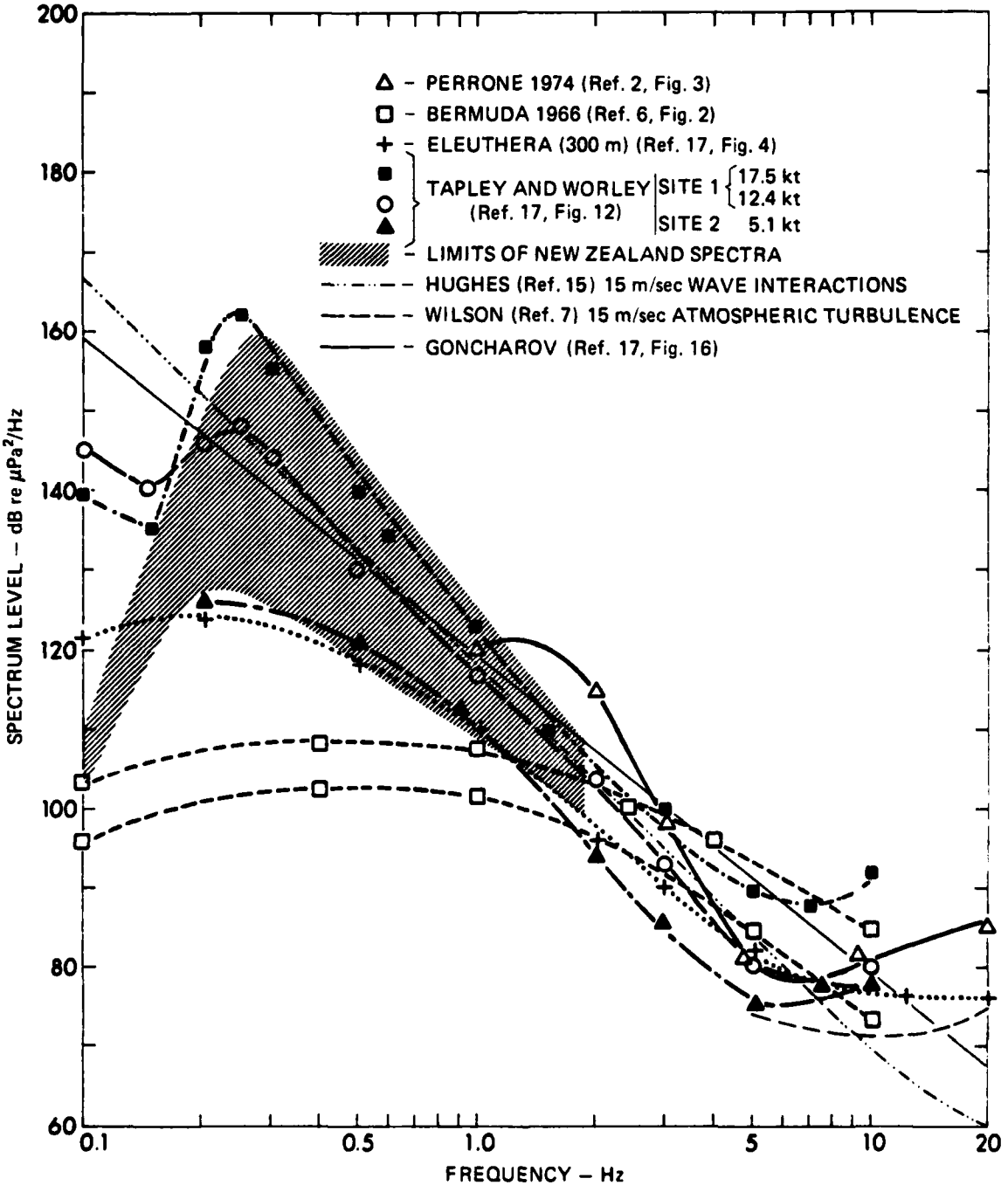

FIGURE 17
COMPARISON OF VARIOUS AMBIENT NOISE DATA SETS

ARL:UT
AS-83-1154
ACK-GA
10-25-83

C. Comparison with Theoretical Predictions

1. Noise Level

The two currently favored theories relating wind and surface waves to ambient noise generation at low frequencies are represented by the papers of Isakovich and Kuryanov[4] and Wilson[7] on the one hand, and Brekhovskikh,[12] Hughes,[14] and Lloyd[15] on the other.

The mechanism proposed by Isakovich and Kuryanov involves the generation of noise by turbulent pressure fluctuations in the atmosphere near the ocean surface. Wilson[7] has recently modified the original theory and used more modern wave height spectral information in computing the noise field. The predicted levels of noise induced by atmospheric turbulence for a wind speed of 15 m/sec (30 kt) are shown in Fig. 17 and to higher frequencies in Fig. 18. In the range of 20 Hz down to 10 Hz, predictions agree reasonably with observations, but below 10 Hz fall below measured values. Wilson concludes that atmospheric turbulence is the dominant source of wind generated noise above 5 Hz and suggests, with others, that surface wave-wave interactions are responsible between 1 and 5 Hz.

Also shown in Figs. 17 and 18 is a noise prediction presented by Nichols[17] (his Fig. 16), based on Goncharov's[16] theory of the interaction of surface waves and ocean turbulence. This is not markedly different from that based on the nonlinear interaction of surface waves alone, but a distinction between the two mechanisms can be drawn on the basis of the frequency characteristics of the noise spectrum (see Subsection 2 below).

Early theoretical estimates of ocean noise generated by nonlinear interactions do not agree closely with measured values either. However, recently Hughes,[14] incorporating modern surface wave data and allowing for surface-bottom reflections, has produced revised estimates. His predicted spectrum for a 15 m/sec wind (extrapolated below 1 Hz) is also shown in Figs. 17 and 18. Below 5 Hz, his predicted values agree closely with the

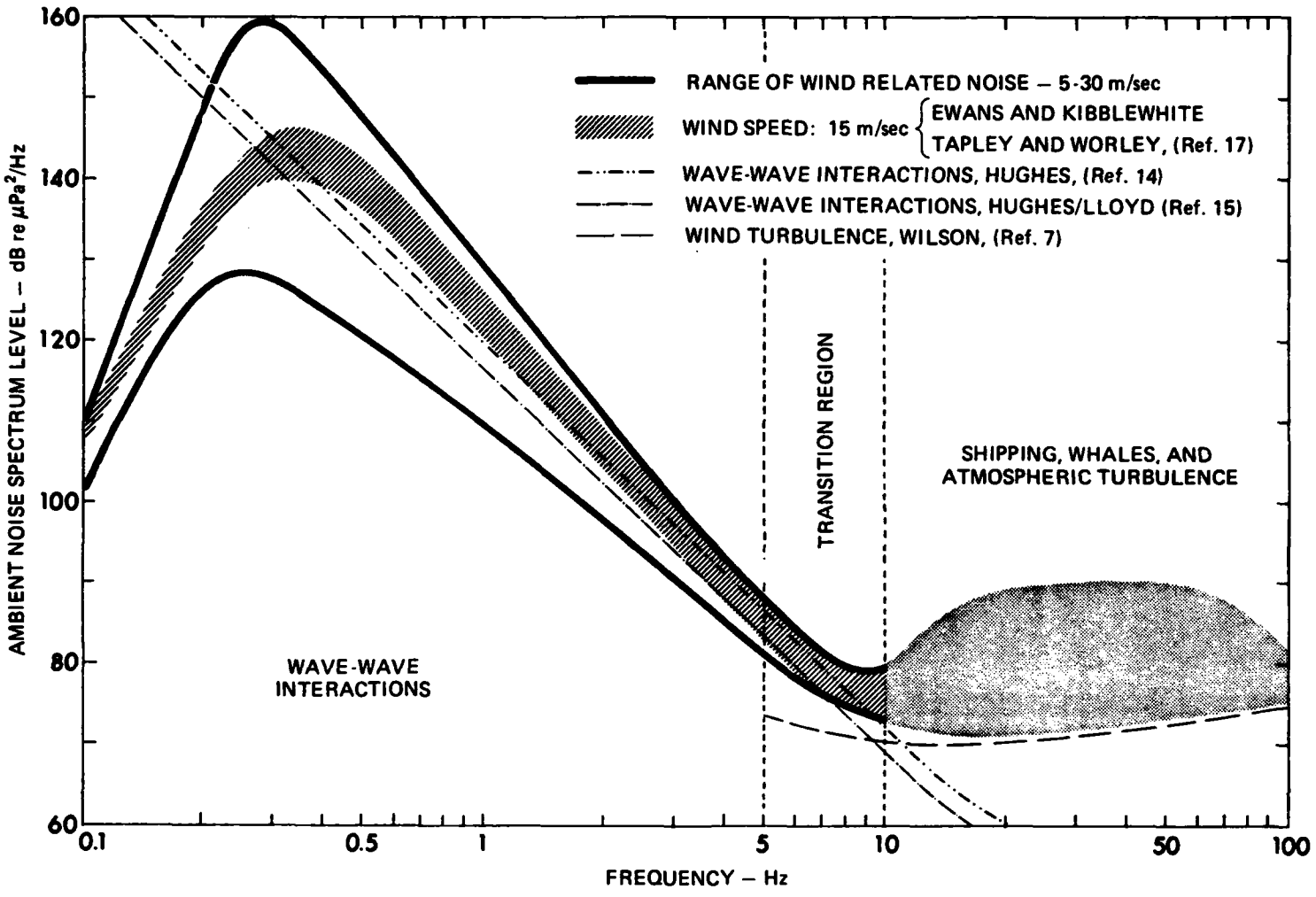

FIGURE 18
SUGGESTED FORM OF THE AMBIENT NOISE SPECTRUM BELOW 100 Hz IN MID-OCEAN WATERS
WIND SPEED: 5-30 m/sec

ARL:UT
AS-83-1155
ACK-GA
10-25-83

Tapley and Worley spectrum (average wind speed of 12.4 kt) and the Maui spectrum of 18 October (1940Z) for which the wind speed was 15 m/sec (30 kt) (see Figs. 16 and 17). Above 10 Hz, the theoretical values fall below the experimental data. It is to be noted, however, that Lloyd has shown Hughes' prediction to be too high by a factor of 2. Hughes' original prediction and Lloyd's amendment are shown in Fig. 18.

At first, the close agreement between the present experimental levels and the theoretical predictions at frequencies below 10 Hz might be seen as fortuitous. The bottom amplification factor included in the theoretical predictions shown in Figs. 17 and 18 (see Ref. 14, Eq. 42) depends upon various parameters, including water depth, and there is uncertainty in assigning values to these parameters appropriate to the Maui area. A bottom reflection coefficient of unity is also assumed, which will not be appropriate to the situation.

It is, however, instructive to compare the acoustic pressure levels derived from the ground displacement with those calculated using the observed values of Sa(f) in Eq. (6). For spectra with a close 2:1 frequency relationship, we find that, at frequencies close to the spectral peak, the two values agree to within a few decibels. At higher frequencies ($0.4 < f < 1.0$ Hz), the pressure levels derived from the wave field are typically 10-15 dB below those deduced from the seismic spectrum.

If we allow a 10-15 dB bottom amplification factor to bring the high frequency levels into agreement, the values near the peak become too high by about the same amount (8-12 dB). Two possible explanations can be considered. The first is that it is not sufficient to only consider the effect of the bottom amplification on the incident pressure field generated by the ocean wave interactions. With a reflection coefficient less than unity, the frequency dependence of the bottom transfer function must be considered. In Eq. (4), a simple frequency dependence was assumed and it is conceivable that an additional frequency dependence is embodied in K_2. An overall frequency dependence of the form required to remove the anomaly between the pressure fields as calculated from Eqs. (2) and (4) is

compatible with what is known of the sedimentary structure in the area. The inflection around 0.5 Hz, apparent in Fig. 15, is suggestive of a transfer function with a narrow peak. Alternatively, it is conceivable that the two equilibrium ranges in the wave spectrum mentioned earlier (see Fig. 15) account for the mismatch between the two frequency regions in the noise spectrum. This would imply that the wave spectral interactions differ in some way in each frequency range, leading to a different power dependence in the frequency parameter in Eq. (6). Certainly nonlinear wave-wave interactions are known to involve primarily frequency components near the spectral peak.[24] It is even possible that a combination of such effects is involved. On the evidence available, it is not possible to resolve the question. It can be noted, however, that recently Burgess and Kewley[37] have shown that ambient noise levels are sensitive to bottom reflectivity.

With the unknowns involved, the quantitative agreement obtained is considered reasonable. It is obvious, however, that the Hughes/Lloyd prediction in Fig. 18 tends to fall below the experimental data (and the predictions based on Eq. (6)) around the spectral peak. It is believed that this arises because of the nature of the wave field in the Maui region. The present study has shown inter alia that a peak enhancement factor, γ, as first discussed by Hasselmann et al.[32] is also necessary for an accurate analytical description of the spectrum of the seas on the west coast of New Zealand.[29,30] The effect of the peak enhancement factor decreases rapidly away from the peak but, at the spectral peak, γ is approximately 2.9 for the Maui seas, so that the pressure field based on Eq. (6) will be greater by a factor of around 10 dB than the Hughes prediction shown in Fig. 18.

In spite of the difficulty with absolute levels, we have additional support for the role of wave-wave interactions below 5 Hz in the theoretical dependence of the observed noise levels on sea state. According to Eq. (2), the acoustic pressure level should be proportional to the second power of the surface wave spectral density (i.e., to $[Sa(\omega)]^2$).

As discussed earlier, this relationship is confirmed by the results of Figs. 10 and 11. Additional evidence is provided by the spectral frequency dependence to be discussed next.

We note finally that, while Wilson's predictions relate to source level, bottom amplification referred to above will have implications for his theoretical curve presented in Figs. 17 and 18. This prediction assumes a seabed of poor reflecting properties and hence no bottom enhancement.[38] With allowance for bottom amplification, Wilson's theoretical curve will be in closer agreement with observed values.

2. Frequency Dependence

Equations (2) and (4) imply that above the peak the frequency dependence of the acoustic noise field (seismic or pressure) depends on the high frequency slope of the ocean wave spectrum. The ratio R_s should however display a fourth or third power dependence on frequency for the ground displacement and acoustic pressure spectra, respectively.

This question was examined earlier and the results of an examination of the ratio R_s using nondimensionalized spectra are given in Table I. It is apparent that, in the region above the spectral peak, the frequency dependence of R_s generally favors the nonlinear wave interaction hypothesis.

Further, the detailed analysis of the nondimensional ocean wave spectra in the Maui region[30] established two intervals in the equilibrium range (Table I and Fig. 15). However, using a mean value of -4.5 for the high frequency slope of the ocean wave field $Sa(\omega)$, one would expect $Sp(2\omega)$ in Eq. (2) to display a frequency dependence of $\omega^3 x \omega^{-9} x \omega^{-6}$, corresponding to a slope of around 18 dB/octave. Figure 16 shows that, at high wind speeds, the spectral slope is of this order between 0.3 and 1 Hz.

Finally, Goncharov's ocean turbulence theory predicts a spectral slope of ω^{-4}. The evidence from spectral slope information therefore

appears to strongly support Brekhovskikh's theory that wave-wave interactions are the noise generating mechanism at frequencies below 5 Hz.

D. Region above 5 Hz

At frequencies between 5 and 10 Hz, another mechanism is obviously beginning to influence the noise level. As Wilson has pointed out, the characteristics of atmospheric turbulence appear to account for the trends observed in this region.

In the absence of any other source, one would expect a minimum in the noise spectrum between 5 and 10 Hz. Such a minimum is apparent in Fig. 17. It is furthermore a definite feature of New Zealand hydrophone data currently being processed and is also strikingly demonstrated in some recent Canadian results (I. Frazer, personal communication).

It is also an observational fact that the energy at very low frequencies is first apparent at 4-5 Hz irrespective of wind speed, but increases rapidly below this frequency. This is another reason for believing that Wilson's theoretical predictions, without a correction for bottom enhancement, will be at least 10-15 dB too low for most regions.

The nature of the spectrum above 5 Hz will however depend on the relative levels of the two wind related noise components, and any shipping and biological activity in the region. The effect these combined sources might be expected to produce on a mid-depth mid-ocean noise spectrum at frequencies below 100 Hz is shown in Fig. 18. At these frequencies, the distortion introduced by volume attenuation will be minor.

X. THE NONLINEAR SOURCE FUNCTION AND NOISE GENERATION

Measurements of wave spectra from various regions, including Maui, indicate an apparent invariance of the nondimensionalized spectral shape. It has been suggested from studies of the spectral energy balance that this can be explained by nonlinear resonant wave-wave interactions. The process not only has a shape stabilizing influence on the spectrum, but is also responsible for the migration of the spectral peak to lower frequencies in a growing wind-sea.[24,32]

In this model, atmospheric input in the central region of the spectrum is balanced by nonlinear energy transfer and leads to rapid adjustment of the spectrum to a quasi-equilibrium level. However, across the peak, the nonlinear source function S_{nl} changes rapidly from positive to negative values (see Fig. 19) and is unable to balance the positive source function for the atmospheric input S_{in}. The imbalance in this region leads to a net transfer of energy in the region of the peak.

Computations of the nonlinear energy transfer for various spectral shapes shows that for a spectrum which is less sharply peaked than the mean JONSWAP spectrum, the low frequency positive lobe of S_{nl} shifts from the forward face of the spectrum to a position immediately below the peak, causing the peak to grow. On the other hand, if the peak becomes narrower, the nonlinear source function develops an additional narrow, positive lobe just to the right of the peak, and the peak broadens again. Thus, the spectrum adjusts to a self-stabilizing form in all cases maintained by nonlinear transfer processes.

It has been shown[34] that the transfer function near the peak is dominated by interactions in which all components of the interacting quadruplets lie in the vicinity of the spectral peak and that the high frequency range of the spectrum is of only minor significance to the evolution and stability of the peak. This property must be, at least in part, responsible for the shape of the microseismic spectra. From all points of view, it is reasonable to conclude that the nonlinear

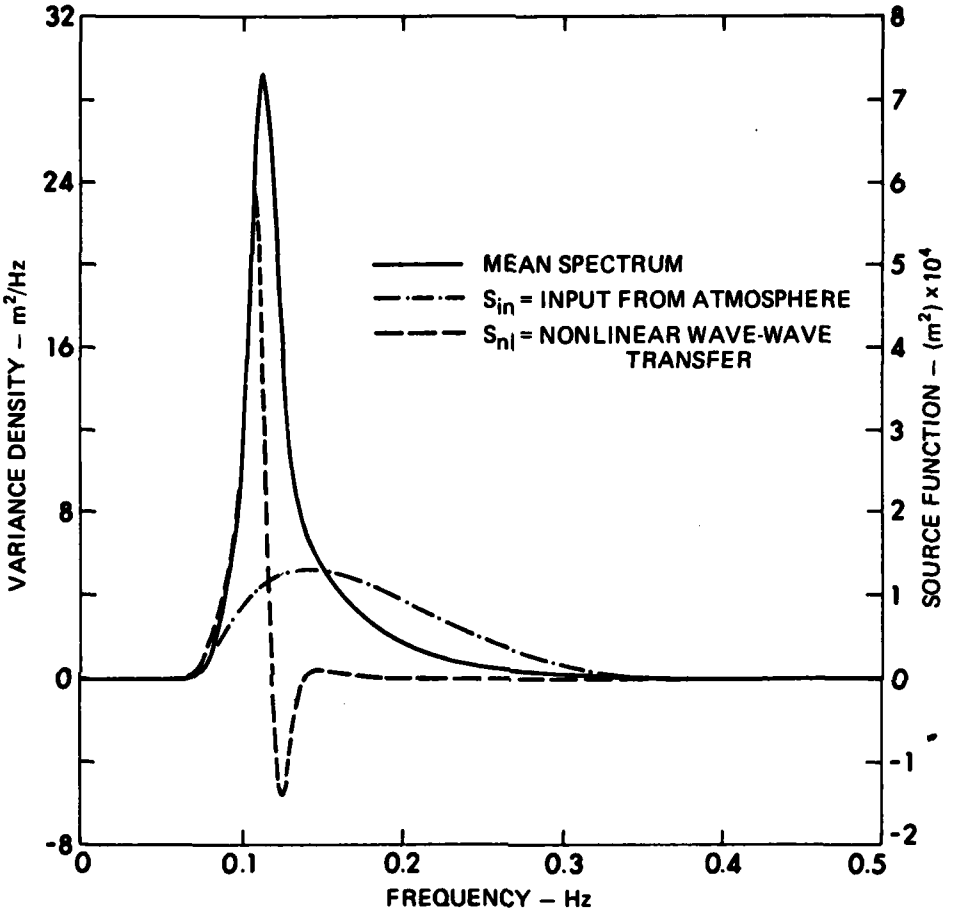

FIGURE 19
MEAN "JONSWAP" SPECTRUM AND SOURCE FUNCTIONS
WIND SPEED: 15 m/sec

ARL·UT
AS-83-1156
ACK · GA
10 · 25 · 83

interactions which stabilize the ocean wave spectrum also generate the acoustic pressure fluctuations and microseism activity observed.

XI. SUMMARY

It has been proposed that nonlinear wave-wave interactions and/or atmospheric turbulent pressure fluctuations provide the most promising explanations for the ocean noise generated in the region below 10 Hz. However, the experimental data covering this part of the spectrum are limited; and, although the evidence is supportive, it has not been possible to provide positive confirmation to date. The main problems arise through the experimental difficulties involved: most noise measurements have been of only short duration and the supporting environmental data have been limited.

An ocean environment possessing particular properties and long term recordings so critical to the resolution of complex geophysical phenomena were features of the present experiment, and it has provided clarification of the roles of the two wind related noise generating mechanisms operating at very low frequencies.

Specifically, it has been demonstrated that surface wave-wave interactions are the dominant mechanism of noise generation from 0.1 to 5 Hz. This mechanism, which is also responsible for the cross-spectral transfer of energy in the wave field and the generation of ocean induced microseisms, clearly plays a major role in ocean wave processes.

It has been shown further why, as has been often observed,[39] the low frequency noise field correlates better with the wind than with sea state and why there is effectively no phase lag. The nonlinear wave interactions which adjust the sea state occur immediately when there is a change in the wind field, but the ocean wave spectrum takes some time to accommodate to the cross-spectral energy transfer.

The noise field is however not a simple function of wind speed. A shift in bearing in a moderate wind field has been shown to have an effect on the sea noise comparable with that produced by a large change in wind speed on a constant bearing. Indeed, several distinct interplays between wind speed and noise level can now be identified.

The greatest wind related noise levels occur when a 180^{o} shift in a wind of long duration brings a growing sea into direct opposition with the one already established. (This effect has been reported before,[40] but its real significance has only been demonstrated with the long term data of the present experiment.) While the two wave fields interact, the noise levels remain very high, but drop quickly to levels some 20 dB lower as the new wave field becomes dominant. This new level of activity reflects the nonlinear processes active within the single wave field and the noise is now related more simply to wind speed.

The processes generating the underwater sound field are those responsible for maintaining the general form of the ocean wave spectrum. As these processes decay with decreasing wind speed, noise levels reach a lower limit set by the same processes active within the residual wave field. This background level will vary from region to region and, in fact, differs by an order of magnitude from the exposed west coast of New Zealand to the quieter seas on the east coast.

Between 5 and 10 Hz, another wind dependent process influences the noise field. The present evidence supports earlier claims that in this frequency region the effects of atmospheric turbulence begin to be manifest. The induced noise field is now related on a 1:1 frequency basis with the fluctuations in the exciting turbulence field and displays different frequency and wind dependent characteristics.

The combined effects of nonlinear interactions and atmospheric turbulence produce a minimum in the noise spectrum around 10 Hz. The visibility of the effects of atmospheric turbulence depends, however, on the influence of shipping and other sources on the noise field.

A close equivalence between seismic levels and the wave induced acoustic levels at the seabed at frequencies below 10 Hz has implications for the modeling of the ocean noise field. In the present experiment, the levels of ground motion recorded by a land based sensor correlated closely with the exciting pressure field. Furthermore, on occasions components in

the seismic spectrum could be correlated with wave activity on the east coast of New Zealand,[27,30] confirming many earlier reports that even in complex geological structures wave induced seismic signals suffer little attenuation in transmission to long distances. The possibility exists, therefore, for energetic storms to influence the noise field at distant regions in the ocean. This possibility is especially marked if the wave interaction occurs on the continental shelf. Downslope propagation as proposed by Wagstaff[41] could in this case occur for any energy reradiated into the water column. The possibility also exists for the equivalent of T-phase transmission transferring energy into the sound channel.

In conclusion, it is of interest to observe that once again the study of a problem in ocean acoustics has been not only dependent on input from oceanography but has also provided a contribution to oceanography. In this case, the properties of the ambient noise field have provided information on mesoscale processes in the ocean wave field.

ACKNOWLEDGMENTS

This investigation was carried out as part of the Maui Development Environmental Study conducted by The University of Auckland for Shell BP and Todd Oil Services, Ltd., acting on behalf of Maui Development, Ltd. Other agencies contributed to the program. In particular, the NZ Meteorological Service provided the weather and wind reports and the University Grants Committee assisted in purchasing some of the specialized instrumentation. The contributions of many individuals are gratefully acknowledged. Special thanks are extended to the staff of the Oaonui Production Station for routine supervision of the recording instrumentation, Mr. P. G. Dolden for maintenance of the wave recorder, and to Dr. M. D. Johns, Mr. D. A. Ash, and Mr. D. B. Coup for computational assistance in analysis. The project could never have been completed successfully, however, without the technical skills and enthusiasm of Mr. D. A. Jones, who not only designed and maintained the shore recording instrumentation, but provided general management support to this and other programs throughout the whole period of the environmental study.

Portions of the analysis and interpretation of this report were carried out while one author (A.C.K.) was associated with Applied Research Laboratories, The University of Texas at Austin. The report is one part of a series of contributions to the understanding of the ambient noise field at very low frequencies. The work was supported by the ARL:UT IR&D fund.

REFERENCES

1. G. M. Wenz, "Acoustic Ambient Noise in the Ocean: Spectra and Sources," J. Acoust. Soc. Am. 34, 1936-1955 (1962).

2. A. J. Perrone, "Infrasonic and Low-Frequency Ambient Noise Measurements on the Grand Banks," J. Acoust. Soc. Am. 55, 754-758 (1974).

3. K. Hasselmann, "A Statistical Analysis of the Generation of Microseisms," Rev. Geophys. 1, 177-210 (1963).

4. M. A. Isakovich and B. F. Kur'yanov, "Theory of Low Frequency Noise in the Ocean," Sov. Phys.-Acoust. 16, 49-58 (1970).

5. W. Strawderman, "Turbulent Air Flow Induced Sea Noise," NUSC Technical Document 12-190-74, Naval Underwater Systems Center, New London, Connecticut, 28 June 1974.

6. N. Yen and A. J. Perrone, "Mechanisms and Modeling of Wind-Induced Low Frequency Ambient Sea Noise," NUSC Technical Report 5833, Naval Underwater Systems Center, New London, Connecticut, 13 February 1979.

7. J. H. Wilson, "Very Low Frequency (VLF) Wind-Generated Noise Produced by Turbulent Pressure Fluctuations in the Atmosphere near the Ocean Surface," J. Acoust. Soc. Am. 66, 1499-1507 (1979).

8. M. Miche, "Mouvements Ondulatoires de la Mer en Profondeur Constante ou Decroissante," Ann. Ponts Chaussees 114, 25-87 (1944).

9. M. S. Longuet-Higgins, "A Theory of the Origin of Microseisms," Philos. Trans. R. Soc. London, Ser. A 243, 1-35 (1950).

10. J. N. Nanda, "The Origin of Microseisms," J. Geophys. Res. 65, 1815-1820 (1960).

11. J. Darbyshire and E. O. Okeke, "A Study of Primary and Secondary Microseisms Recorded in Anglesey," Geophys. J. R. Astr. Soc. 17, 63-92 (1969).

12. L. M. Brekhovskikh, "Underwater Sound Waves Generated by Surface Waves in the Ocean," Izv. Atmos. Ocean. Phys. 2, 582-587 (1966). (Translated by J. Gollob.)

13. E. Y. Harper and P. G. Simpkins, "On the Generation of Sound in the Ocean by Surface Waves," J. Sound Vib. 37, 185-193 (1974).

14. B. Hughes, "Estimates of Underwater Sound (and Infrasound) Produced by Nonlinearly Interacting Ocean Waves," J. Acoust. Soc. Am. 60, 1032-1039 (1976).

15. S. P. Lloyd, "Underwater Sound from Surface Waves according to the Lighthill-Ribner Theory," J. Acoust. Soc. Am. 69, 425-435 (1981).

16. V. V. Goncharov, "Sound Generation in the Ocean by the Interaction of Surface Waves and Turbulence," Izv. Atmos. Ocean. Phys. 6, 1189-1196 (1970). (Translated by F. Goodspeed.)

17. R. H. Nichols, "Infrasonic Ambient Ocean Noise Measurements: Eleuthera," J. Acoust. Soc. Am. 69, 974-981 (1981).

18. F. I. Monakhov and V. M. Zhak, "The Mechanism of Microseism Generation from the Sea-Floor Observations off the Island of Shikotan," Izv. Earth Phys. 13(4), 290-292 (1977).

19. F. I. Monakhov, V. M. Zhak, and V. A. Nesterov, "Mechanism of Generation of Microseism by a Storm during the Period October 10-11, 1976, near Island Shikotan," Izv. Earth Phys. 14(4), 302-303 (1978).

20. A. A. Ostrovsky, "On Some Characteristics of Microseism Sources," Izv. Earth Phys. 15(11), 825-828 (1979).

21. G. V. Latham and A. I. Mowroozi, "Waves, Weather and Ocean-Bottom Microseisms," J. Geophys. Res. 73, 3945-3957 (1968).

22. G. H. Sutton, W. G. McDonald, D. D. Prentiss, and S. N. Thanos, "Ocean-Bottom Seismic Observations," Proc. IEEE 53, 1909-1921 (1965).

23. R. J. Urick, "Sea-Bed Motion as a Source of Ambient Noise Background in the Sea," J. Acoust. Soc. Am. 56, 1010-1011 (1974).

24. K. Hasselmann, D. B. Ross, P. Muller, and W. Sell, "A Parametric Wave Prediction Model," J. Phys. Ocean. 6, 200-228 (1976).

25. D. O. Zopf, H. C. Creech, and W. H. Quinn, "The Wavemeter: A Land-Based System for Measuring Nearshore Ocean Waves," Mar. Tech. Soc. J. 10(4), 19-25 (1976).

26. A. C. Kibblewhite and R. N. Denham, "Experiment on Sound Propagation in Shallow Water under Isovelocity Conditions," J. Acoust. Soc. Am. 40, 1337-1344 (1966).

27. A. C. Kibblewhite, P. R. Bergquist, B. A. Foster, M. R. Gregory, and M. C. Miller, "Maui Development Environmental Study: Report on Phase 2, 1977-1981," University of Auckland, New Zealand, October 1982.

28. S. M. Chiswell and A. C. Kibblewhite, "Ocean Wave Studies in Western Cook Strait," NZ J. Mar. Freshwater Res. 14(4), 417-425 (1980).

29. S. M. Chiswell and A. C. Kibblewhite, "Spectra of the Fully Developed Wind Generated Ocean Wave Field West of Central New Zealand," NZ J. Mar. Freshwater Res. 15(1), 81-84 (1981).

30. K. C. Ewans, "Ocean Waves, Microseisms, and Their Interrelations," Doctoral Dissertation, University of Auckland, New Zealand, 1984.

31. M. S. Longuet-Higgins, "On the Statistical Distribution of Heights of Sea Waves," J. Mar. Res. 11(3), 245-266 (1952).

32. K. Hasselmann, J. P. Barnett, E. Bouws, H. Carlson, D. E. Cartwright, K. Enke, J. A. Ewing, H. Glenapp, D. E. Hasselmann, P. Kruseman, A. Meerburg, P. Muller, D. J. Olbers, K. Richter, W. Sell, and H. Walden, "Measurements of Wind-Wave Growth and Swell Decay during the Joint North Sea Wave Project (JONSWAP)," Dent. Hydrogr. Z. Suppl. A, 8, No. 12 (1973).

33. G. M. Hidy and E. J. Plate, "Frequency Spectrum of Wind-Generated Waves," Phys. Fluids 8, 1387-1389 (1965).

34. P. C. Liu, "Normalized and Equilibrium Spectra of Wind Waves in Lake Michigan," J. Phys. Ocean. 1(4), 249-257 (1971).

35. G. Z. Forristall, "Measurements of a Saturated Range in Ocean Wave Spectra," J. Geophys. Res. 86, 8075-8084 (1981).

36. G. L. Tyler, C. C. Teague, R. H. Stewart, A. M. Peterson, W. H. Munk, and J. W. Joy, "Wave Directional Spectra from Synthetic Aperture Observations of Radio Scatter," Deep Sea Res. 21, 989-1016 (1974).

37. A. S. Burgess and D. J. Kewley, "Wind-Generated Surface Noise Source Levels in Deep Water East of Australia," J. Acoust. Soc. Am. 73, 201-210 (1983).

38. J. H. Wilson, "Wind-Generated Noise Modeling," J. Acoust. Soc. Am. 73, 211-216 (1983).

39. J. A. Shooter and M. L. Gentry, "Wind Generated Noise in the Parece Vela Basin," J. Acoust. Soc. Am. 70, 1757-1761 (1981).

40. V. N. Tabulevich, "Swell, Opposing Winds and Microseisms," Izv. Geophys. Ser. No. 11, 1667-1675 (1963).

41. R. A. Wagstaff, "Low Frequency Ambient Noise in the Deep Sound Channel--The Missing Component," J. Acoust. Soc. Am. 69, 1009-1013 (1981).

16 August 1984

DISTRIBUTION LIST FOR
ARL-TR-84-2

Copy No.

Commanding Officer
Naval Ocean Research and Development Activity
NSTL, MS 39529
1 Attn: E. D. Chaika (Code 270)
2 R. Gardner (Code 201)
3 D. B. King (Code 321)
4 W. A. Kuperman (Code 220)
5 R. Martin (Code 110A)
6 J. Matthews (Code 362)
7 W. W. Worsley (Code 110A)

Chief of Naval Research
Department of the Navy
Arlington, VA 22217
8 Attn: M. McKisic (Code 4250A)
9 R. Obrochta (Code 425AR)

Office of Naval Research Detachment
Naval Ocean Research and Development Activity
NSTL, MS 39529
10 Attn: G. Morris (Code 425GG)
11 LCDR M. McDonald (Code 425GG)

Commanding Officer
Naval Electronic Systems Command
Department of the Navy
Washington, DC 20360
12 Attn: LCDR S. Hollis (Code 612)
13 R. Mitnick (Code 612)
14 CDR C. Spikes (PDE 124-60)
15 L. Parish (PDE 124-50)

Director
Naval Research Laboratory
Department of the Navy
Washington, DC 20375
16 Attn: B. B. Adams (Code 8160)

Distribution List for ARL-TR-84-2 (Cont'd)

Copy No.

Commanding Officer
Naval Ocean Systems Center
Department of the Navy
San Diego, CA 92152

17 Attn: E. L. Hamilton
18 M. A. Pederson
19 H. P. Bucker

Commander
Naval Sea Systems Command
Department of the Navy
Washington, DC 20362

20 Attn: C. D. Smith (Code 63R)
21 D. E. Porter (Code 63R1)

Chief of Naval Operations
Department of the Navy
Washington, DC 20360

22 Attn: CAPT E. Young (OP 952D)

Chief of Naval Material
Department of the Navy
Washington, DC 20360

23 Attn: CAPT J. Harlett (MAT 0724)

24 Commander
Naval Surface Weapons Center
White Oak Laboratory
Department of the Navy
Silver Spring, MD 20910

25 Commander
David W. Taylor Naval Ship Research and
Development Center
Department of the Navy
Bethesda, MD 20034

Naval Oceanographic Office
Department of the Navy
NSTL, MS 39522

26 Attn: W. Jobst (Code 7300)
27 J. Allen (Code 7310)
28 R. Hecht (Code 7332)

Distribution List for ARL-TR-84-2 (Cont'd)

Copy No.

Commander
Naval Air Development Center
Department of the Navy
Warminster, PA 18974
29 Attn: C. L. Bartberger

Officer in Charge
New London Laboratory
Naval Underwater Systems Center
Department of the Navy
New London, CT 06320
30 Attn: B. Cole
31 F. R. DiNapoli
32 P. Herstein

33 Director Naval Warfare
Deputy Undersecretary Defense R&E
Room 3D1048, Pentagon
Washington, DC 20301

OASN (R,E&S)
Room 4D745, Pentagon
Washington, DC 20301
34 Attn: G. A. Cann

Superintendent
Naval Postgraduate School
Monterey, CA 93940
35 Attn: Library

Commander
Naval Coastal Systems Center
Department of the Navy
Panama City, FL 32407
36 Attn: G. McLeroy

Defense Advanced Research Projects Agency
1400 Wilson Blvd.
Arlington, VA 22209
37 Attn: CDR K. Evans (TTO)

38 Commander
Naval Intelligence Support Center
4301 Suitland Road
Washington, DC 20390

Distribution List for ARL-TR-84-2 (Cont'd)

Copy No.

39 - 50	Commanding Officer and Director Defense Technical Information Center Cameron Station, Building 5 5010 Duke Street Alexandria, VA 22314	
	Woods Hole Oceanographic Institution 86-95 Water Street Woods Hole, MA 02543	
51	Attn:	T. Brocher, Dept. of Geology & Geophysics
52		R. Spindel
	Science Applications, Inc. 1710 Goodridge Drive McLean, VA 22101	
53	Attn:	C. Spofford
54		J. Hanna
	Science Applications, Inc. 9760 Owensmouth Avenue Chatsworth, CA 91311	
55	Attn:	J. H. Wilson
	Applied Research Laboratory The Pennsylvania State University P. O. Box 30 State College, PA 16801	
56	Attn:	S. McDaniel
	Marine Physical Laboratory of The Scripps Institution of Oceanography The University of California, San Diego San Diego, CA 92132	
57	Attn:	F. Fisher
58		G. Shor
	Scripps Institution of Oceanography The University of California, San Diego La Jolla, CA 92093	
59	Attn:	Library
60		R. Adair, A-008
61		R. Tyce

Distribution List for ARL-TR-84-2 (Cont'd)

Copy No.

Bell Telephone Laboratories, Inc.
Whippany Road
Whippany, NJ 07961
62 Attn: A. Carter
63 R. Holford
64 D. Romain

Bell Telephone Laboratories
Summit, NJ 07901
65 Attn: S. P. Loyd

Planning Systems, Inc.
7900 Westpark Drive, Suite 507
McLean, VA 22101
66 Attn: R. Cavanaugh
67 B. Brunson

TRW, Inc.
TRW Defense & Space Systems Group
Washington Operations
7600 Colshire Drive
McLean, VA 22101
68 Attn: R. T. Brown
69 I. Gereben

Defence Scientific Establishment
HMNZ Dockyard
Devonport, Auckland
NEW ZEALAND
70 Attn: Director
71 K. M. Guthrie

Defence Scientific Establishment
Naval Post Office
Auckland, NEW ZEALAND
72 Attn: Scientist-in-Charge

School of Mechanical Engineering
Georgia Institute of Technology
Atlanta, GA 30332
73 Attn: A. D. Pierce

Distribution List for ARL-TR-84-2 (Cont'd)

Copy No.

Department of Geology and Geophysics
Geophysical and Polar Research Center
Lewis G. Weeks Hall for Geological Sciences
The University of Wisconsin, Madison
1215 W. Dayton Street
Madison, WI 53706
74 Attn: C. S. Clay

Courant Institute
251 Mercer Street
New York, NY 10012
75 Attn: D. C. Stickler

Bolt, Beranek, & Newman, Inc.
50 Moulton Street
Cambridge, MA 02138
76 Attn: H. Cox

Hawaii Institute of Geophysics
The University of Hawaii
2525 Correa Road
Honolulu, HI 96822
77 Attn: L. N. Frazer

Director
North Atlantic Treaty Organization
SACLANT ASW Research Centre
APO New York 09019
78 Attn: T. Akal

Defence Research Establishment, Pacific
FMO Victoria, BC
VOS 1BO CANADA
79 Attn: R. Chapman

Defence Research Establishment, Atlantic
9 Grove Street
P. O. Box 1012
Dartmouth, Nova Scotia
CANADA BZY 3Z7
80 Attn: D. Chapman
81 I. A. Frazer

Distribution List for ARL-TR-84-2 (Cont'd)

Copy No.

Rosenteil School of Marine and
Atmospheric Science
The University of Miami
10 Rickenbacker Causeway
Miami, FL 33149
82 Attn: H. DeFarrari

Applied Physics Laboratory
The Johns Hopkins University
Johns Hopkins Road
Laurel, MD 20810
83 Attn: J. Lombardo
84 R. Henrick

Department of Ocean Engineering
Massachusetts Institute of Technology
Cambridge, MA 02139
85 Attn: I. Dyer
86 G. Duckworth
87 A. Baggerar

The University of Miami
10 Rickenbacker Causeway
Miami, FL 33149
88 Attn: F. Tappert

Physics Department
The University of Rhode Island
Kingston, RI 02881
89 Attn: C. Kaufman

Department of Electrical Engineering
Polytechnic Institute of New York
Farmingdale, NY 11735
90 Attn: L. B. Felsen

91 I. Tolstoy
Knockvennie, Castle Douglas
S. W. SCOTLAND
GREAT BRITAIN

Department of Geology
The University of Texas at Austin
Austin, TX 78713
92 Attn: C. Wilson

Distribution List for ARL-TR-84-2 (Cont'd)

Copy No.

Physics Department
The University of Auckland
Private Bag, Auckland
NEW ZEALAND
93 Attn: A. C. Kibblewhite
94 C. T. Tindle
95 K. C. Ewans

Chinhae Research Laboratory
P. O. Box 18
Chinhae, Kyeong Nam
KOREA
96 Attn: Jungyul Na

The Lamont-Doherty Geological Observatory
Columbia University
Palisades, NY 10964
97 Attn: R. D. Stoll

Ocean Data Systems, Inc.
Defense Systems
6110 Executive Blvd., Suite 320
Rockville, MD 20852
98 Attn: G. Jacobs
99 P. C. Etter

Tetra Tech Services, Inc.
3559 Kenyon Street
San Diego, CA 92110
100 Attn: Donald Ross

Butler Service Group
16 Main Street
Madison, NJ 07940
101 Attn: R. H. Nichols

102 Nancy R. Bedford, ARL:UT

103 Karl C. Focke, ARL:UT

104 Robert F. Gragg, ARL:UT

105 Loyd Hampton, ARL:UT

106 Kenneth E. Hawker, ARL:UT

Distribution List for ARL-TR-84-2 (Cont'd)

Copy No.	
107	Stephen G. Houser, ARL:UT
108	Jo B. Lindberg, ARL:UT
109	Robert A. Koch, ARL:UT
110	David Knobles, ARL:UT
111	Stephen K. Mitchell, ARL:UT
112	David W. Oakley, ARL:UT
113	Clark S. Penrod, ARL:UT
114	Carol V. Sheppard, ARL:UT
115	Jack A. Shooter, ARL:UT
116	Paul J. Vidmar, ARL:UT
117	Library, ARL:UT
118 - 128	Reserve, ARL:UT